Mineralogical Magazine, May 2018, Vol. 82(S1), pp. S281–S306

Trace-element geochemistry of molybdenite from porphyry Cu deposits of the Birgilda-Tomino ore cluster (South Urals, Russia)

Olga Y. Plotinskaya[1,*], Vera D. Abramova[1], Elena O. Groznova[1,2], Svetlana G. Tessalina[3], Reimar Seltmann[4] and John Spratt[4]

[1] Institute of Geology of Ore Deposits, Petrography, Mineralogy, and Geochemistry Russian Academy of Sciences (IGEM RAS), Staromonetny per. 35, Moscow 119017, Russia

[2] Institute of Experimental Mineralogy Russian Academy of Sciences (IEM RAS), Chernogolovka, Moscow region 142432, Russia

[3] John de Laeter Centre for Isotope Research & The Institute for Geoscience Research (TIGeR), Curtin University, Kent St, Bentley, WA 6102, Australia

[4] Natural History Museum, London SW7 5BD, UK

[*Received 16 January 2017; Accepted 23 December 2017; Associate Editor: Krister Sundblad*]

ABSTRACT

Mineralogical, electron microprobe analysis and laser ablation-inductively coupled plasma-mass spectrometry data from molybdenite within two porphyry copper deposits (Kalinovskoe and Birgilda) of the Birgilda-Tomino ore cluster (South Urals) are presented.† The results provide evidence that molybdenites from these two sites have similar trace-element chemistry. Most trace elements (Si, Fe, Co, Cu, Zn, Ag, Sb, Te, Pb, Bi, Au, As and Se) form mineral inclusions within molybdenite. The Re contents in molybdenite vary from 8.7 ppm to 1.13 wt.%. The Re distribution within single molybdenite flakes is always extremely heterogeneous. It is argued that a temperature decrease favours the formation of Re-rich molybdenite. The high Re content of molybdenite observed points to a mantle-derived source.

Keywords: molybdenite, LA-ICP-MS, porphyry copper deposits, Urals.

Introduction

Porphyry copper deposits are the major source of Re as a by-product (Dill, 2010) and molybdenite is the only economically significant carrier of this element. Rhenium is currently ranked as a critical metal in very short supply in Russia (Trach and Beskin, 2011), making the study of the rhenium distribution in known deposits very relevant. For this reason porphyry copper deposits of the Urals have recently attracted attention as potential sources of both molybdenum and rhenium. General features of rhenium distribution in Uralian porphyry copper deposits were discussed by Grabezhev (2013) while the rhenium behaviour of individual deposits and within single grains of molybdenite has been described recently (e.g. Grabezhev and Shagalov, 2010; Grabezhev and Gmyra, 2014; Grabezhev and Hiller, 2015; Grabezhev and Voudouris, 2015; Plotinskaya *et al.*, 2014*a*, 2015). Among the numerous porphyry deposits and occurrences known in the Urals (Plotinskaya *et al.*, 2017*a*,*b*)

*E-mail: plotin-olga@yandex.ru

†The term 'ore cluster' is used here, and in previous publications, to mean an irregular group of ore deposits that occupy an area larger than an ore field and do not form an alignment or trend.

https://doi.org/10.1180/minmag.2017.081.106

This paper is part of a special open access issue in the Mineralogical Magazine entitled 'Critical-metal mineralogy and ore genesis'.

the area of the Birgilda-Tomino ore cluster is one of the most interesting due to a remarkable variability of styles of mineralization (Plotinskaya *et al*., 2014*b*) and it is economically promising because of the large Tomino porphyry copper deposit. The rhenium distribution in molybdenite from the Tomino deposit was described by Grabezhev and Hiller (2015).

The present study has provided new mineralogical, electron microprobe analysis (EMPA) and laser ablation inductively coupled plasma mass spectrometry (LA-ICP-MS) data from molybdenite from two porphyry copper deposits of the Birgilda-Tomino ore cluster, Kalinovskoe and Birgilda. The main goal of this paper is to describe, at the scale of single molybdenite flakes, the distribution of rhenium and other trace elements as well as to discuss the controls of this distribution.

Geological background

The general geology and tectonic setting of the Birgilda-Tomino ore cluster were described in detail by Puzhakov (1999), Grabezhev *et al*. (1998) and Plotinskaya *et al*. (2014*b*, 2017*a*,*b*). The ore cluster is located within the East-Uralian Volcanic Terrane (the shaded area in the inset of Fig. 1*a*) which is interpreted as a series of fragments of intra-oceanic arcs of Silurian to Devonian age (Yazeva and Bochkarev, 1995; Samygin and Burtman, 2009; Puchkov, 2017). The northeastern part of the area (Fig. 1*a*) comprises the Early to Middle Ordovician Sargazy Formation with a maximum thickness of 1500 m. It is composed of aphyric basalt and andesitic basalt supplemented by minor porphyric basalt and basaltic volcanoclastic rocks, as well as rhyolite and rhyolite tuffs metamorphosed to greenschist facies (Puzhakov, 1999). This formation hosts all known porphyry copper deposits in this area. In the central part of the area, the Sargazy basalts are overlain by Middle Ordovician to Lower Silurian limestones and marbles of the Biksizak Formation that host the Biksizak base-metal carbonate replacement deposit. The Sargazy basalts and the Biksizak Formation are overlain in turn by volcanics of the Bereznyakovskoe Formation which hosts epithermal Au-Ag deposits and occurrences, including the Bereznyakovskoe ore field. The Bereznyakovskoe Formation comprises andesitic dacite volcanoclastic rocks up to 1000 m thick and minor andesitic dacite lavas with rare limestone interlayers (Grabezhev *et al*., 1998; Puzhakov, 1999). Younger sediments include Upper Silurian to Middle Devonian limestone, Givetian to Famennian sediments (siltstones, schists, sandstones with minor limestone), Visean volcanics, and Visean to Moscovian terrigenous-carbonate sequences (Puzhakov, 1999). Numerous diorite and andesite porphyry stocks of the Birgilda–Tomino Igneous Complex, dated as 428 ± 3 Ma and 427 ± 6 Ma (Grabezhev *et al*., 2013), are believed to have produced both porphyry and epithermal-style mineralization (Grabezhev *et al*., 1998; Puzhakov, 1999). The Chelyabinsk Pluton, located in the northernmost part of the area, comprises several Late Devonian to Permian intrusive phases (Kallistov, 2014).

The Kalinovskoe deposit

The Kalinovskoe porphyry copper deposit (Fig. 1*b*) together with the neighbouring Tomino deposit and several smaller occurrences make up the Tomino porphyry copper ore field. Porphyry-style mineralization is confined to a large stock, ~2 km in diameter, composed of quartz diorite, amphibole plagioclase diorite and porphyritic varieties, which belong to the Birgilda-Tomino Igneous Complex. The mineralization occurs both in diorites and in hosting Ordovician basalts. In the central zones of the diorite stocks, phyllic alteration accompanies chalcopyrite ± bornite ± molybdenite mineralization, while in the peripheral zone, propylitic alteration dominates with pyrite-chalcopyrite mineralization and occasional magnetite and hematite. The latest-stage mineralization, which occurs in the periphery of the Kalinovskoe deposit, includes various Bi-sulfosalts (bismuthinite–aikinite series, matildite), native gold, galena, sphalerite, tetrahedrite (Plotinskaya *et al*., 2014*b*) with bornite, chalcopyrite and rare Au-Ag, Ag, Pb, Bi, and Hg tellurides. The oxidation zone is up to 40 m thick and contains malachite, azurite and chalcocite. The total reserves (Russian A + B + C categories) of the Tomino and Kalinovskoe deposits make up 331 Mt at 0.46 wt.% Cu and 0.1 g/t Au (Volchkov *et al*., 2015). Grabezhev (2013) reported Cu/Mo ratios from 100 to 300, but Mo occasionally rises to 3–80 ppm which decreases the Cu/Mo ratios to 25–50.

The Birgilda deposit

The Birgilda deposit (Fig. 1*c*) was the first porphyry-style mineralization discovered in the area

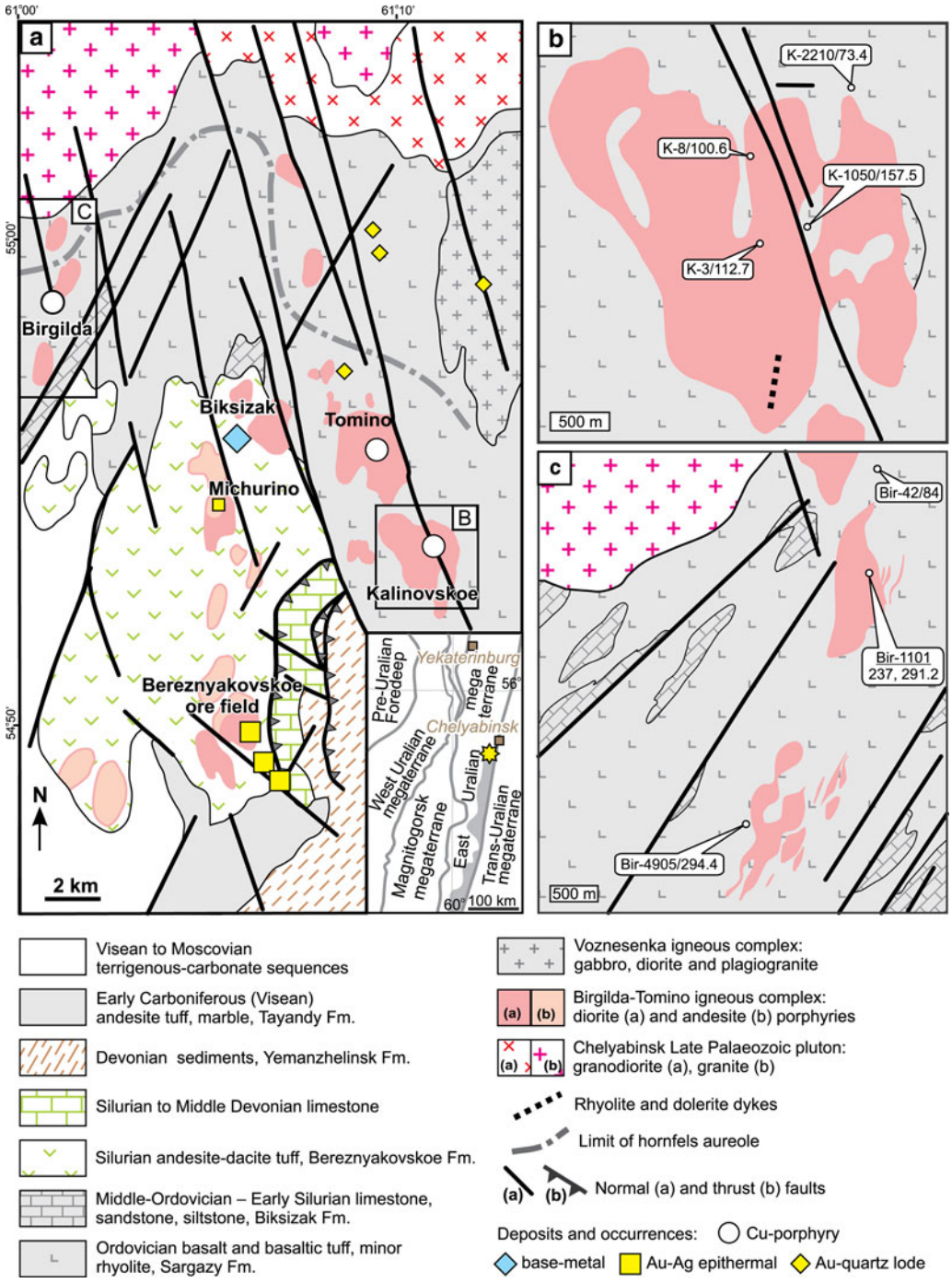

FIG. 1. Geological maps of the Birgilda-Tomino ore cluster: (*a*) the Kalinovskoe deposit, modified after Grabezhev *et al*. (2000); (*b*) modified after Chelyabinskgeolsiomka JSC and Puzhakov (1999); (*c*) The Birgilda deposit, simplified after Narykova *et al*. (2015). The inset in (*a*) shows the East-Uralian volcanic terrane highlighted in grey and the yellow star indicates the position of the Birgilda-Tomino ore cluster.

(Romashova, 1984). The mineralization is associated with two stocks of diorite and diorite porphyry known as South and North Birgilda, respectively; each ~1 km in size. The diorites are altered pervasively to quartz-sericite (phyllic) and mixed chlorite-sericite, while propylitic (chlorite ± epidote) alteration dominates in the host basalts. Pyrite, chalcopyrite and molybdenite are the main ore minerals. Both the mineralization and the alteration are similar to those at Kalinovskoe. The Birgilda deposit was reported by Pravda (2015) to contain 152.2 kt of Cu at 0.51 wt.% Cu. Grabezhev and Belgorodskii (1992) noted a Cu/Mo ratio of 150.

Molybdenite assemblages and sampling

Molybdenite occurs in both study areas as μm- to mm-scale nests, usually in white to grey quartz veinlets or, sometimes, disseminated in the host rocks. It occurs mainly within the diorite intrusions where it is accompanied by quartz + sericite ± chlorite alteration, but it is also observed in the host basalt. Molybdenite is always associated with chalcopyrite, chlorite, sometimes with pyrite, white mica, and, occasionally, with epidote and carbonate.

Molybdenite-bearing samples were collected from exploration drill cores. Samples were selected for EMPA and LA-ICP-MS analysis to represent both the central and the peripheral zones of the deposits studied (Fig. 1*b*,*c*) as well as from diorite and basalt host rocks. A detailed description of both samples is given in Table 1 and images in Figs 2 and 3. The two most molybdenite-rich samples (K-3/112.7 and Bir-1101/237) were selected for Re-Os dating.

Analytical methods

Re-Os dating of molybdenite

Molybdenite-bearing samples were crushed and grains intergrown with molybdenite were hand-picked using a needle under a binocular microscope. Molybdenite-rich separates (~25 to 30 mg) were transferred into Carius tubes resting in dry ice, followed by the addition of a mixed ^{188}Os-^{190}Os/^{185}Re spike as recommended by Markey *et al*. (2003) and digested in 'inverted *aqua regia*'. The sealed tubes were placed in an oven at 220°C and allowed to react for 48 h. Osmium was separated by solvent extraction, with a final purification of Os by microdistillation. Rhenium was separated from a portion of the residual liquid using anion exchange chromatography. Isotopic measurements were made by means of a Thermo-Ionization Mass-Spectrometer (TIMS) Triton™ instrument using the Faraday collectors for both Re and Os. Measured Os isotope ratios were first corrected for contributions from natural Os (based on preliminary isotope dilution calculations), then corrected for mass fractionation based on the ^{190}Os/^{188}Os ratio of the spike. ^{187}Os was determined from the ^{187}Os/^{188}Os ratio of the mixture and corrected for minor contributions from total common Os (blank plus sample). Most of the error in both the Re and Os concentrations is from the uncertainties of the spike calibrations and the mass spectrometric measurements, an error magnification factor, uncertainties on blank corrections and, for the age determination, uncertainty in the decay constant for ^{187}Re. The weighing error of the sample does not contribute to the uncertainty in the ages because of a mixed-double ^{188}Os-^{190}Os/^{185}Re spike used (Markey *et al*., 2003). Analytical blanks are insignificant for the age calculations, given the Re and ^{187}Os concentrations of the samples studied and the sample size used in the analyses. Blank values were 1 pg/g for Re and 4 pg/g for Os with ^{187}Os/^{188}Os of 0.15. The uncertainty for each individual age determination does not exceed 0.5%, including the 0.3% uncertainty in the decay constant of ^{187}Re.

EMPA study

The chemical compositions of ore and gangue minerals were determined using a Zeiss EVO 15LS scanning electron microscope with an Oxford Instruments X-Max EDX detector (Natural History Museum, London) using the following beam conditions: beam diameter 1–2 μm, accelerating voltage 20 kV, beam current 3 nA, and a counting time of 20 s. The 1σ analytical error was 0.06–0.08 for Mn and Cr and did not exceed 0.2 wt.% for all other elements. The detection limit was accepted as 1σ.

The molybdenite composition was determined using a Cameca SX-100 electron microprobe with five WDX spectrometers (Natural History Museum, London, UK). X-ray mapping using Re*L*α, Re*M*α, Mo*L*α, S*K*α, Ca*K*α, Si*K*α, Fe*K*α, and Zn*K*α was carried out first, and points for single spot analysis were then selected from the resulting X-ray map data.

For the Kalinovskoe deposit the operating conditions were: beam diameter 1–2 μm,

TABLE 1. Molybdenite-bearing samples selected for this study.

Sample No	Sample description	Molybdenite morphology and assemblage
Kalinovskoe deposit		
K-3/ 112.7*	Microdiorite with greyish quartz veinlet; numerous stringers of chalcopyrite and molybdenite (Fig. 2*a*).	Aggregate of irregularly oriented molybdenite flakes, ~2 mm× 3 mm in size, in a quartz veinlet. Individual flakes are from 10–30 to 100–200 μm long, intergrown with chlorite (Fig. 2*b*).
K-1050/ 157.5	Veinlet of greyish quartz with nests of molybdenite and chalcopyrite in axial parts and carbonate in selvages; the host rock is diorite porphyry altered to quartz-sericite-chorite metasomatite (Fig. 2*c*)	Aggregate of irregularly oriented molybdenite flakes, ~100 mm × 70 μm in size, in a quartz veinlet. Intergrown with chalcopyrite, chlorite, calcite (Fig. 2*d*).
K-8/ 100.6	Light-grey quartz veinlet with carbonate nests in quartz-chlorite-sericite rock. Large nests of pyrite and magnetite in the axial zone, chloritization in selvages (Fig. 2*e*)	Molybdenite flake, ~200 μm × 100 μm, slightly deformed and split to μm-scale flakes. Intergrown with chlorite, calcite and epidote (Fig. 2*f*).
K-2210/ 73.4	Quartz-sericite rock with abundant nests of molybdenite and chalcopyrite (Fig. 2*g*). Molybdenite from the subset of this sample was dated by the Re-Os method as 431.7 ± 1.7 Ma (Tessalina and Plotinskaya, 2017))	Molybdenite nest ~0.8 × 2 mm composed of flakes up to 500 μm in size. Intergrown with pyrite and chalcopyrite. Matildite overgrowths on chalcopyrite and molybdenite (Fig. 2*h*). Quartz, chlorite, minor albite, epidite and titanite are gangue minerals.
Birgilda deposit		
Bir-1101/237	Diorite cut by a small plagiogranite dyke, both with intense quartz-sericite-chlorite alteration; both are cut by a white-grey quartz veinlet with molybdenite in selvages (Fig. 3*a*).	Molybdenite 'semi-rosette' 1–0.3 mm in size located on the border of a quartz veinlet and albite-chlorite-sericite altered diorite. Composed of molybdenite flakes from 10 to 50 μm wide and 100 to 200 μm long. Intergrown with chlorite, quartz, albite, minor muscovite, K-feldspar and chalcopyrite. (Fig. 3*b*,*c*)
Bir-1101/ 291.2	Aphyric basalt with pervasive chlorite alteration and numerous epidote-pyrite stringers; veinlet of white quartz with large pyrite nests and small nests of molybdenite (Fig. 3*d*).	Aggregate of irregularly oriented molybdenite flakes in conjunction with pyrite aggregate in a quartz veinlet. Individual flakes are from 10–30 to 80 μm wide and 50 to 150 μm long, intergrown with quartz, epidote, albite, K-feldspar, albite, chalcopyrite (Fig. 3*e*,*f*).
Bir-4905/ 294.4	Quartz-sericite-chlorite rock with abundant nests of black tourmaline; veinlet of light grey quartz with molybdenite in selvages and pyrite nest in axial zone (Fig. 3*g*).	Molybdenite 'semi-rosette' 250 μm × 150 μm in size located on the border of quartz veinlet and carbonate-quartz-sericite altered rock. Molybdenite flakes are ~20–30 μm wide and 50 to 150 μm long. Intergrown with chlorite, muscovite, quartz and calcite (Fig. 3*h*).
Bir-42/ 84	Aphyric basalt with pervasive chlorite alteration and epidote-pyrite stringers and nests; quartz veinlet with pyrite, magnetite and chalcopyrite.	Aggregate of irregularly oriented molybdenite flakes from 2–3 to 10 μm wide and up to 50 μm long, intergrown with epidote, titanite, rutile, chlorite and albite (Fig. 3*i*).

* Drill hole number/depth in m.

accelerating voltage 20 kV, beam current 20 nA, and analytical lines Re$L\alpha$, Mo$L\alpha$, Zn$L\alpha$ and S$K\alpha$. Counting time was: 60 s for S, 120 s for Zn, 240 s for Mo, and 240 s for Re. The peak overlaps were corrected for 0.002% Mo/S and 0.04% S/Mo. The detection limits were (wt.%): 0.06 for S, 0.03 for Re and Zn and 0.02 for Mo. Standard deviation was (wt.%): 0.33 for S, 0.03 for Re, 0.02 for Zn and 0.40 wt. for Mo.

For the Birgilda deposit the conditions were: beam diameter 1–2 μm, accelerating voltage 20 kV, beam current 40 nA, and analytical lines Si$K\alpha$,

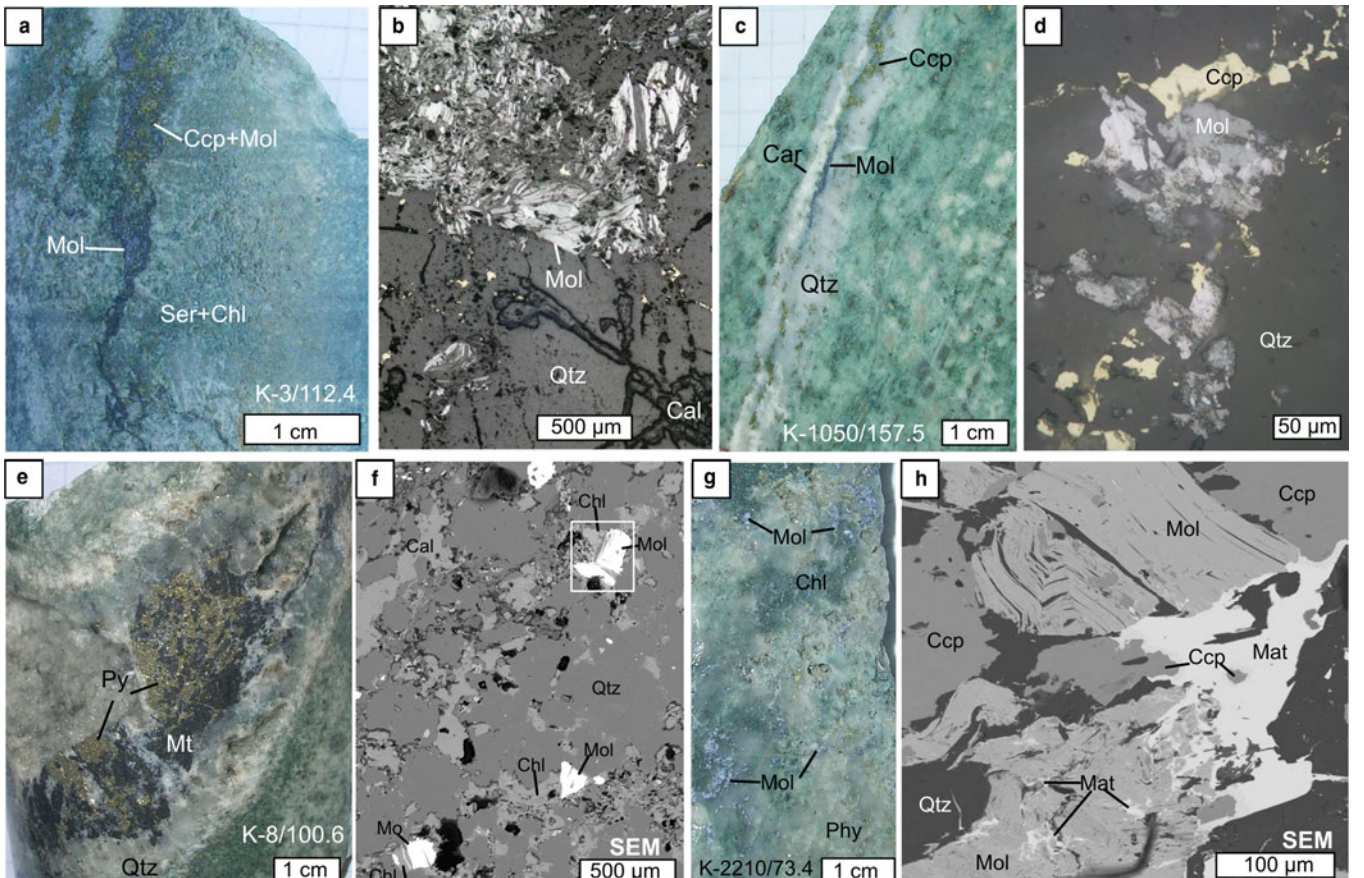

FIG. 2. Molybdenite from Kalinovskoe: (*a*,*b*) sample K-3/112.7, molybdenite (Mol) and chalcopyrite (Ccp) in quartz (Qtz) veinlet in a sericite-chlorite (Ser + Chl) rock; (*c*, *d*) sample K-1050/157.5, molybdenite and chalcopyrite cutting a quartz veinlet in an altered diorite; (*e*,*f*) sample K-8/100.6, pyrite (Py) and magnetite (Mt) in a quartz veinlet with minor molybdenite; (*g*,*h*) sample K-2210/73.4, quartz-sericite altered (Phy) diorite with nests of molybdenite; (*h*) molybdenite intergrown with chalcopyrite and overgrown by matildite (Mat). 'SEM'– scanning electron microscope images; (*a,c,e,g*) – hand specimens; (*b,d*) – reflected light images.

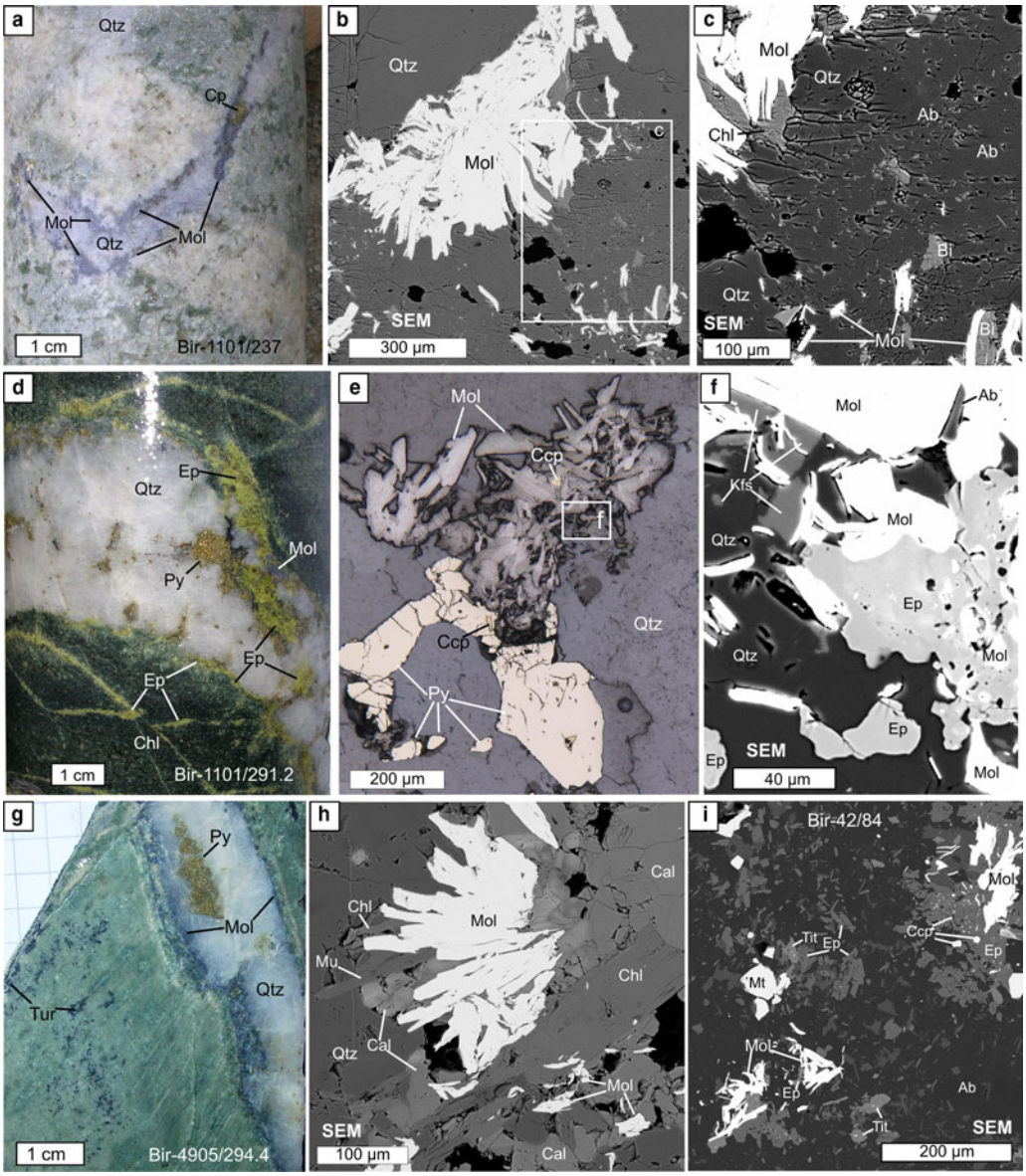

FIG. 3. Molybdenite (Mol) from Birgilda: (*a*–*c*) sample Bir-1101/237, molybdenite nests intergrown with chlorite, albite (Ab) and biotite (Bi) in selvages of a quartz veinlet; (*d*–*f*) sample Bir-1101/291.2, molybdenite intergrown with pyrite, chalcopyrite, epidote (Ep), albite and K-feldspar (Kfs); (*g*,*h*) sample Bir-4905/294.4, molybdenite overgrown by calcite (Cal), muscovite (Mu) and chlorite; (*i*) sample Bir-42/84, molybdenite flakes in basalt altered to an albite, epidote assemblage with magnetite, titanite (Tit) and chalcopyrite. 'SEM' – scanning electron microscope images; (*a*,*d*,*g*) – hand specimens; (*e*) – reflected light images.

S*Kα*, Fe*Kα*, Zn*Lα*, Se*Lα*, Mo*Lα*, Te*Lα*, Re*Lα*, W*Lα*. The counting time was: 20 s for Si and Zn, 30 s for Se, 100 s for Mo, and 120 s for S, Fe, Te, Re and W. The data were corrected for peak overlaps as following: 85.04% for Re/Zn, 4.16% for Mo/S, 0.35% for Zn/Mo, 0.16% for Si/Re, 0.14% for W/Re, 0.18% for W/Zn, 0.07% for W/Mo, −0.14% for S/Mo and −0.12% for Re/Mo. The

TABLE 2. Re-Os ages and abundance results for the molybdenite samples studied.

Sample	Re (ppm)	±2σ	^{187}Re, (ppm)	±2σ	^{187}Os (ppb)	±2σ	Model age (Ma)	±2σ (Ma)
K-3/112.7	198.6	0.6	124.8	0.4	901.2	0.1	431.9	1.9
Bir-1101/237	583.2	1.4	366.6	0.9	2647.5	0.2	432.0	1.7

detection limits were (wt.%): 0.04 for Re, S, Mo, and W, 0.05 for Zn, 0.03 for Fe, 0.02 for Se and Te, 0.01 for Si. Standard deviation was (wt.%): 0.04 for Re and Zn, 0.61 for S, 0.38 for Mo, 0.03 for W, 0.02 for Fe, Se and Te, and 0.01 for Si. The following reference materials were used: metallic Fe, W, Re and Mo, fayalite for Si, PbSe for Se, BiTe for Te and sphalerite for Zn and S.

LA-ICP-MS study

The trace-element data for molybdenite were acquired using the LA-ICP-MS system at IGEM RAS (Moscow). The LA-ICP-MS consists of a New Wave 213UP laser coupled with the Thermo X Series2 quadrupole ICP-MS. The following isotopes were measured Si^{29}, S^{33}, Fe^{57}, Co^{59}, Ni^{60}, Cu^{65}, Zn^{66}, As^{75}, Se^{77}, Mo^{95}, Ag^{107}, Sn^{118},Sb^{121}, Te^{125}, W^{182}, Re^{185}, Re^{187}, Au^{197}, Pb^{208} and Bi^{209}. For external calibration the following standard reference materials (SRM) were used: in-house pyrrhotite standard $Fe_{0.9}S$, synthesized using the method of Wohlgemuth-Ueberwasser *et al.* (2007) and calibrated with respect to concentration of elements against standards at UQAC (Sylvester *et al.*, 2005) for Fe, Ag, Re, Au; MASS-1 polymetal sulfide (USGS) for the remaining elements and ^{33}S was used as the internal standard based on molybdenite stoichiometry. GSE, a synthetic basalt glass with 25 wt.% Si, was used for Si calibration and verification of the other results with Mo as the internal standard. LA-ICP-MS analyses of external standards and molybdenite samples were conducted at the same conditions using a 40 to 60 μm diameter spot size, a laser frequency of 15 Hz, 5–7 mJ input power and 5 μm/s ablation speed for profiles. Acquisition time in spot mode was 30 s for the background and 30 s for the mineral analysis. The washout time was 30 s between measuring individual laser spots. All standards were run before and after each set of 15 unknowns as well as before and after each set of 40 and 60 μm spot sizes. LA-ICP-MS data were processed using the *Iolite* data-reduction software, v. 2.5 (Paton *et al.*, 2011).

Fluid-inclusion study

Microthermometric measurements of fluid inclusions were carried out on doubly polished thin sections using a LINKAM THM-600 heating-freezing stage at the Institute of Experimental Mineralogy Russian Academy of Sciences, Chernogolovka. The temperature of phase transitions was measured over the range –196 to +600°C with an accuracy of ±0.2°C between –20°C and +20°C and no less than ±1.0°C outside of this interval. The salt composition of the fluids was determined from the eutectic temperature (T_e) according to Crawford (1981); the salinity was estimated from the temperature of ice melting (T_m) using the NaCl–H_2O phase diagram (Bodnar and Vityk, 1994). The measurements were carried out for groups of inclusions with similar relationships of phases to avoid errors related to the disintegration of vacuoles after fluid heterogenization (Roedder, 1984). Pressure was calculated using the method proposed by Kaluzhny (1982) for coexisting fluid inclusions of CO_2 and water–salt composition using diagrams from Thiery *et al.* (1994) and the *FLINKOR* software (Brown, 1989).

Results

Re-Os ages of molybdenite

For the Kalinovskoe and the Birgilda deposits, the molybdenite samples yielded Re-Os ages of 431.9 ± 1.9 and 432.0 ± 1.7 Ma respectively (Table 2). The uncertainty of the individual age determination for both samples is in the order of 0.4%.

Molybdenite chemistry

Kalinovskoe deposit

The EMPA study revealed Re contents above the detection limit in three of the four samples from the Kalinovskoe deposit (Table 3 and Supplementary Material – Appendix 1). From those, the totals of only 41 analyses out of 100 were >98 wt.% because the molybdenite flakes were either too small or too

TABLE 3. Summary EMPA data for trace elements in molybdenite (wt.%).

Sample	Comment		Re	Si	Fe
Kalinovskoe deposit					
K-3/112.7	Aggregate of irregularly oriented molybdenite flakes, ~2 mm × 3 mm in	Min	<dl	n.a.	n.a.
n = 71	size, in a quartz veinlet. Individual flakes are from 10–30 to 100–200 μm	Max	0.95		
	long, intergrown with chlorite, phengite, muscovite, paragonite, calcite,	Mean	0.31		
	TiO_2.	Median	0.31		
		SD	0.21		
K-1050/	Aggregate of irregularly oriented molybdenite flakes, ~100 μm × 70 μm in	Min	0.09	n.a.	n.a.
157.5	size, in a quartz veinlet. Intergrown with chalcopyrite, chlorite,	Max	0.95		
n = 8	muscovite, paragonite, calcite.	Mean	0.42		
		Median	0.35		
		SD	0.31		
K-8/100.6	Molybdenite flake, ~200 μm × 100 μm in size, slightly deformed and split	Min	<dl	n.a.	n.a.
n = 14	to μm-scale flakes. Intergrown with chlorite, paragonite, epidote.	Max	0.17		
		Mean	0.08		
		Median	0.07		
		SD	0.05		
Birgilda deposit					
Bir-1101/	Molybdenite 'semi-rosette' 1 mm × 0.3 mm in size located on the border of	Min	<dl	0.05	<dl
237	a quartz veinlet and albite-chlorite-sericite altered diorite. Composed of	Max	0.56	1.56	1.57
n = 27	molybdenite flakes 10–50 μm wide and 100–200 μm long. Intergrown	Mean	0.22	0.20	0.13
	with chlorite, quartz, albite, and chalcopyrite.	Median	0.16	0.06	0.02
		SD	0.16	0.34	0.34
Bir-1101/	Aggregate of irregularly oriented molybdenite flakes in conjunction with	Min	0.29	0.05	<dl
291.2	pyrite aggregate in a quartz veinlet. Individual flakes are from 10–30 to	Max	1.13	4.30	0.10
n = 49	80 μm wide and 50–150 μm long, intergrown with epidote, albite,	Mean	0.61	0.20	0.02
	K-feldspar, albite, chalcopyrite.	Median	0.55	0.08	0.02
		SD	0.23	0.61	0.01
Bir-4905/	Molybdenite 'semi-rosette' 250 μm × 150 μm in size located on the border	Min	<dl	<dl	<dl
294.4	of a quartz veinlet and carbonate-quartz-sericite altered rock.	Max	0.21	0.15	0.29
n = 40	Molybdenite flakes are ~20 μm –30 μm wide and 50 to 150 μm long.	Mean	0.09	0.06	0.07
	Intergrown with chlorite, phengite, quartz, and calcite.	Median	0.09	0.05	0.04
		SD	0.04	0.03	0.07
Bir-42/84	Aggregate of irregularly oriented molybdenite flakes from 2–3 to 10 μm	Min	0.04	n.a.	n.a.
n = 15	wide and up to 50 μm long intergrown with epidote, titanite, rutile,	Max	0.20		
	chlorite, and albite.	Mean	0.12		
		Median	0.12		
		SD	0.05		

A full set of individual analyses is given in Appendix 1.<dl – below the detection limit; n.a. – not analysed.

thin. Significant negative correlation was noted between the Re and Mo contents in analyses with a total >99 wt.% (r = –0.56, *n* = 22) confirming substitution of Mo by Re.

X-ray mapping using the Re$L\alpha$ line combined with point analyses revealed an uneven rhenium distribution in all of the molybdenite flakes and, moreover, different distribution patterns in different samples. In sample K-8/100.6 (Fig. 4*a*,*b*) a deformed molybdenite flake has an elevated Re content in the central part (0.06 to 0.08 wt.%) and marginal zones (up to 0.17 wt.%) while the Re content of the remaining part of the flake is below the detection limit. In sample K-1050/157.5 (Fig. 4*c*,*d*), Re-rich molybdenite (up to 0.95 wt.% Re) overgrows Re-poor molybdenite (up to 0.1 wt.% Re). In sample K-3/112.7 (Fig. 4*e*,*f*) in a large aggregate of molybdenite flakes, high Re contents (~0.2 to 0.95 wt.%) form linear zones (up to dozens of μm wide) on the margins of the flakes, or, occasionally spots. K-2210/73.4 is the only sample where the Re contents are below the detection limit.

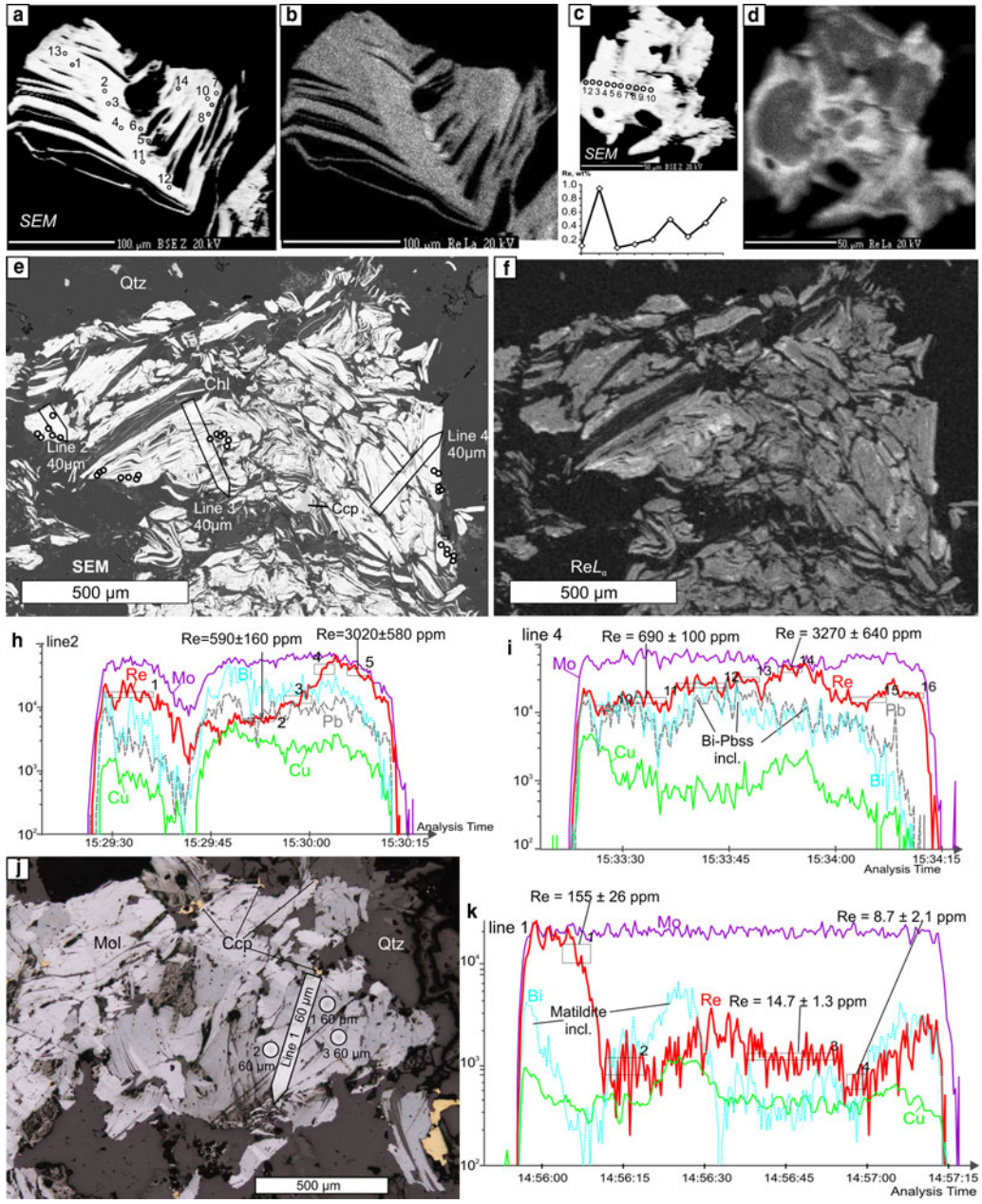

FIG. 4. Molybdenite from Kalinovskoe: (*a*,*b*) sample K-8/100.6, (*a*) SEM image of a deformed molybdenite flake showing the locations of the EMPA analyses; (*b*) Re*L*α X-ray map of the same area; (*c*,*d*) sample K-1050/157.5, (*c*) SEM image of a molybdenite flake with EMPA profile, (*d*) Re*L*α X-ray map; (*e*–*i*) sample K-3/112.7 – (*e*) SEM image of a molybdenite aggregate with the positions of the EMPA analyses and the LA-ICP-MS profiles, (*f*) Re*L*α X-ray map of the same area; (*h*,*i*) the LA-ICP-MS spectra for the profiles 2 and 4, respectively; (*j*) sample K-2210/73.4 with positions of the LA-ICP-MS analyses and profiles; (*k*) LA-ICP-MS spectra for line 1.

TABLE 4. Summary of molybdenite chemistry (LA-ICP-MS data); the full data are presented in Appendix 2.

Sample	(ppm)	Fe	Si	Co	Ni	Cu	Zn	As	Se	Sn	Sb	Te	Re	W	Au	Pb	Bi	Ag
Kalinovskoe site																		
K-3/112.7	Min	<dl	<dl	1	<dl	59	15	<dl	32	<dl	0.3	<dl	302	<dl	<dl	4.7	2.0	8.3
$n = 16$	Max	34,900	12,400	48	35	7900	420	50	350	2.7	3.5	92	4540	1.4	21.3	106.0	155.0	104.0
	Median	2720	1205	18	–	1105	114	26	157	–	1.1	29	1660	–	3.0	71.0	67.0	44.5
	Geom. mean	2654	972	13	–	932	96	21	133	–	1.2	22	1569	–	2.9	48.4	46.6	40.8
	SD	10,654	4231	13	–	2346	114	15	99	–	0.9	31	1320	–	6.4	30.5	43.2	29.0
K-2110/74.3	Min	<dl	n.a.	<dl	<dl	94	6	39	118	<dl	<dl	<dl	8.7	1.4	<dl	0.9	2.3	2.1
$n = 7$	Max	2950	–	5.7	–	2140	24	79	234	–	–	–	1144	4.3	–	9.7	115.0	20.2
	Median	–	–	–	–	119	10	59	195	–	–	–	125	3.0	–	1.5	19.8	4.0
	Geom. mean	–	–	–	–	250	12	55	181	–	–	–	75	2.6	–	2.5	16.9	5.4
	SD	–	–	–	–	772	8	14	40	–	–	–	411	1.0	–	3.4	45.0	6.6
Birgilda site																		
Bir-1101/291.2	Min	30	<dl	<dl	<dl	6.8	26	30	90	<dl	<dl	<dl	3350	12.2	<dl	1.97	0.15	<dl
$n = 11$	Max	3250	3630	1.6	7.1	2780	277	58	238	1.1	3.3	–	7500	42.5	1.2	10.4	4.4	9.7
	Median	310	430	–	–	84	80	47	170	–	0.75	–	5800	22.9	–	4.6	0.9	4.5
	Geom. mean	314	350	–	–	86	83	45	157	–	0.8	–	5272	22.2	–	4.2	0.9	3.8
	SD	945	1060	–	–	815	66	9	55	–	1.1	–	1444	8.0	–	2.6	1.3	3.0
Bir-4905/294.5	Min	240	<dl	<dl	<dl	35	16	34	213	<dl	0.9	<dl	998	5.3	<dl	5.5	1.8	2.7
$n = 13$	Max	3780	940	1.7	–	3200	255	104	540	1.5	33	12.0	1570	12.8	0.7	55.0	13.3	8.5
	Median	990	430	0.9	–	459	37	57	310	–	5.3	–	1203	8.8	–	26.0	5.8	5.9
	Geom. mean	1158	378	0.9	–	387	44	61	300	–	5.6	–	1199	9.2	–	20.1	5.1	5.6
	SD	1187	258	0.4	–	1155	70	24	86	–	9.8	–	156	2.1	–	14.8	3.2	1.9
Bir-1101/237	Min	78	140	<dl	<dl	13	44	45	364	<dl	<dl	<dl	1220	3.3	<dl	4.5	1.8	1.3
$n = 12$	Max	1720	1360	–	–	410	209	79	600	3.0	3.9	–	3240	15.8	–	99.0	27.1	10.2
	Median	335	495	–	–	37	75	70	555	1.1	1.2	–	2330	5.0	–	13.4	5.6	4.3
	Geom. mean	323	456	–	–	37	83	67	521	1.2	1.2	–	2241	5.5	–	13.9	5.7	4.8
	SD	443	386	–	–	110	52	10	72	0.8	1.2	–	690	3.3	–	26.6	7.4	2.9

n – number of intervals within LA-ISP-MS profiles selected for calculation; Geom. mean = geometrical mean; dl = detection limit; the values below dl were treated as half dl in the statistical analysis; statistical parameters were not calculated for those datasets where more than half of the values were below dl; n.a. = not analysed.

TABLE 5. Correlation coefficients for trace elements in molybdenite from the Kalinovskoe site inferred from LA-ICP-MS data: significant* correlation coefficients are highlighted in bold.

	Fe	Co	Cu	Zn	Ag	Sb	Te	Au	Pb	Bi	As	Se	W	Re
Fe	1													
Co	**0.77**	1												
Cu	**0.44**	**0.57**	1											
Zn	**0.86**	**0.85**	0.27	1										
Ag	0.31	**0.68**	**0.73**	0.42	1									
Sb	0.25	**0.70**	0.17	**0.58**	**0.59**	1								
Te	0.13	**0.53**	**0.69**	0.21	**0.88**	0.44	1							
Au	0.30	**0.55**	**0.79**	0.23	**0.77**	0.24	**0.80**	1						
Pb	0.39	**0.84**	**0.62**	**0.58**	**0.88**	**0.81**	**0.73**	**0.67**	1					
Bi	0.32	**0.57**	**0.78**	0.24	**0.74**	0.23	**0.72**	**0.73**	**0.64**	1				
As	**–0.47**	**–0.49**	**–0.46**	**–0.53**	**–0.46**	–0.35	–0.30	**–0.47**	**–0.53**	–0.21	1			
Se	–0.31	–0.19	0.21	–0.41	0.10	–0.14	0.23	0.20	–0.07	0.18	0.13	1		
W	–0.36	**–0.55**	–0.37	**–0.53**	**–0.52**	**–0.52**	**–0.46**	–0.37	**–0.59**	–0.31	**0.59**	0.14	1	
Re	0.10	0.17	0.05	0.32	0.16	0.34	0.02	–0.04	0.28	–0.05	**–0.51**	–0.27	**–0.64**	1

*Minimum significant correlation was accepted as 0.42 for $n = 23$ for 95% confidence, after (Fisher and Yates, 1963).

In addition Grabezhev and Hiller (2015) reported Re contents as high as 0.05 to 0.07 wt.% in four of 130 point analyses of the subset of this sample.

Molybdenite grains large enough to be analysed by LA-ICP-MS were observed only in samples K-3/112.7 and K-2210/73.4. In both samples, molybdenite shows highly variable trace-element concentrations (Table 4 and Supplementary Material – Appendix 2). Both samples show very high Fe contents (up to 34,900 ppm) and Cu (up to 7900 ppm), while sample K-3/112.7 also has a high Si content (up to 12,400 ppm), probably due to intergrowths with chalcopyrite and silicates. Both samples have up to several hundred ppm of Zn, Se and tens of ppm of As, Pb, Bi and Ag (Table 4). The contents of Co, Ni, Sn, Sb, Te and Au are below the detection limit in sample K-2210/73.4 but reach several ppm to tens of ppm in sample K-3/112.7. The opposite is true for W which is up to 4 ppm in sample K-2210/73.4 and mainly below the detection limit in sample K-3/112.7. The maximum Re content in sample K-3/112.7 is 4540 ppm which is in good agreement with the EMPA data (Fig. 4*h*,*i*). In sample K-2210/73.4 Re varies from 9 to 1144 ppm with a geometric mean of 75 ppm, in general agreement with the data of Tessalina and Plotinskaya (2017) who measured 81.5 ppm of Re within the same sample.

Pearson's correlation coefficients were calculated for the whole dataset of trace elements except for Ni and Sn as these elements are below detection limit in more than a half of all analyses (Table 5). There is a significant positive correlation between Fe, Co, Cu, Zn, Ag, Sb, Te, Au, Pb and Bi. In addition, in sample K-3/112 there is a strong positive correlation between Si and Fe, Co and Zn (0.85, 0.78 and 0.88, respectively, at minimum significant 0.5 for $n = 16$). Arsenic and W, in contrast, have negative correlations with most trace elements but a positive correlation with each other (0.59). Re has negative correlations with W and As and no correlation with other elements. Se doesn't have either positive or negative correlations with any trace elements.

Birgilda deposit

The EMPA study revealed Re contents above the detection limit in most analyses of all four samples from the Birgilda deposit (Table 3 and Supplementary Material – Appendix 1). The totals were >98 wt.% in 107 of 140 analyses due to the small grain size.

X-ray mapping using the Re$L\alpha$ line revealed an uneven distribution of Re in all the molybdenite flakes (Figs 5–7). In all four samples, Re-enriched zones encompass areas from several μm across in sample Bir-42/84 (Fig. 5*a*,*b*) to tens of μm wide (samples Bir-1101/237 and Bir-1101/291.2) and up to hundreds of μm long (Figs 6 and 7). These zones are confined to either axial or marginal parts of molybdenite flakes but are always parallel to the

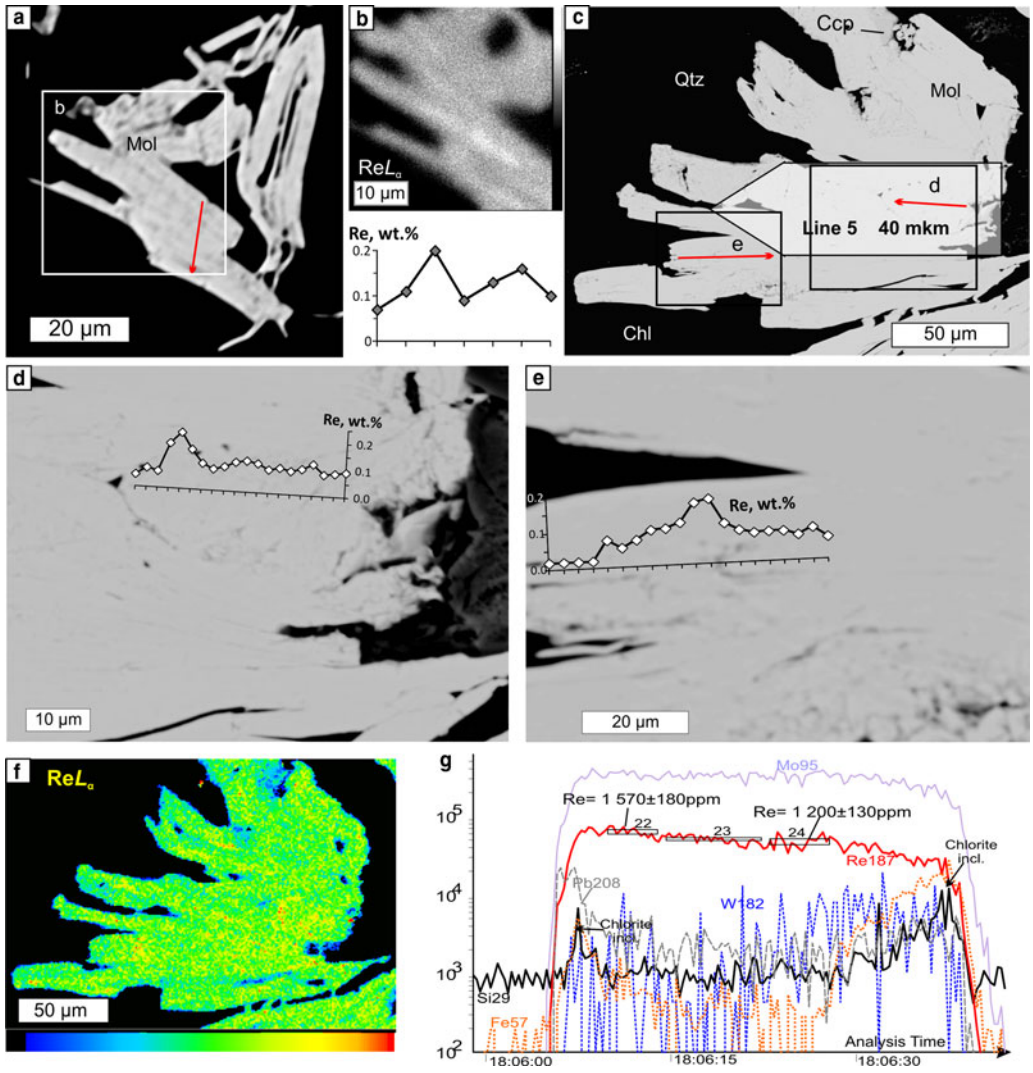

FIG. 5. Molybdenite from Birgilda, samples Bir-42/84 (*a*,*b*) and Bir-4905/294.4 (*c*). (*a*) SEM image of molybdenite flakes; (*b*) Re*L*α X-ray map of a fragment of *a* and the EMPA profile across the flake (the position is indicated by a red arrow); (*c*) SEM image of a molybdenite 'semi-rosette' with the positions of the EMPA and LA-ICP-MS profiles; (*d*,*e*) fragments of (*c*) with the EMPA profiles; (*f*) Re*L*α X-ray map of (*c*); (*g*) LA-ICP-MS spectra for line 5.

elongation of molybdenite flakes. In contrast, in sample Bir-4905/294.4 (Fig. 5*c–f*), Re is confined to several less clearly defined zones which are μm wide and tens of μm long striking across molybdenite flakes. The largest Re contents (0.29–1.13 wt.%) were detected in sample Bir-1101/291.2 while the smallest (0.04–0.21 wt.%) were recorded in sample Bir-4905/294.4 (Table 3).

LA-ICP-MS analysis was carried out for three samples from the Birgilda deposit where molybdenite aggregates were large enough, i.e. Bir-1101/237, Bir-1101/291.2 and Bir-4905/294.4 (Table 4 and Supplementary Material – Appendix 2). Similar to molybdenite from the Kalinovskoe deposit, the Fe, Cu and Si contents reach thousands of ppm because of numerous inclusions of silicates and chalcopyrite. The Co, Ni, Sn, Te and Au contents are below the detection limit in most analyses but occasionally reach several ppm. All samples show similar ranges of Zn, As, Se (tens to a few hundreds

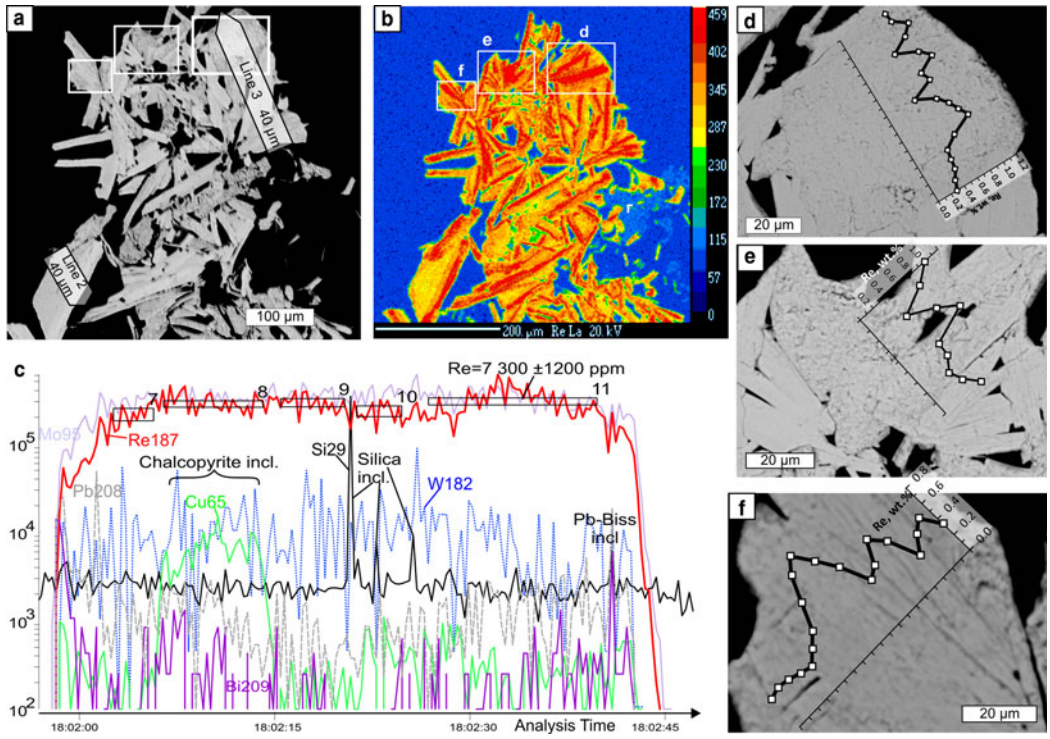

FIG. 6. Molybdenite from Birgilda, sample Bir-1101/291.2: (*a*) SEM image of a molybdenite aggregate showing the positions of the LA-ICP-MS profiles; (*b*) Re*L*α X-ray map of the same area; (*c*) LA-ICP-MS spectra for line 3; (*d–f*) fragments of (*a*) with EMPA profiles.

of ppm), Ag, Pb, Bi and W (several ppm to a few tens of ppm). Sample Bir-4905/294.4 has the highest Sb content (up to 33 ppm compared to <4 ppm in the two other samples). Sample Bir-1101/291.2 is notable for the highest Re content (3350 to 7500 ppm) while the lowest Re content is observed in sample Bir-4905/294.4 (998–1570 ppm) which corresponds with the EMPA data.

Pearson's correlation coefficients were calculated for the entire trace-elements dataset except for Co, Ni, Sn, Te and Au because those elements were below the detection limit in more than a half of the analyses (Table 6). The highest positive correlations (>0.9) exist between Fe and Cu and between Pb and Bi. The Birgilda deposit is similar to the Kalinovskoe deposit with most trace elements showing positive correlations with each other, i.e. Si, Fe, Cu, Zn, Ag, Sb, As, Se, Pb and Bi. Rhenium has negative correlations with Pb, Sb, Bi, Se and As, while W has negative correlations with Se and As. For the Birgilda deposit, the calculation (Table 6) indicates a positive correlation (0.55) between Re and W. However, on a Re *vs.* W diagram (Fig. 8*a*), samples Bir-4905/294.4 and Bir-1101/237 and sample Bir-1101/291.2 clearly form two distinct trends each of which shows a significant negative correlation between Re and W (–0.62 for sample Bir-1101/291.2). This demonstrates that the W and Re behaviour in molybdenite from the Birgilda deposit is similar to that from the Kalinovskoe deposit. Despite the negative correlation between Re and Se for molybdenite from the Birgilda deposit (Fig. 8*b*), there is a positive Re *vs.* Se correlation for analyses with Re <2500 ppm (+0.64 at minimum significant 0.44, $n = 20$) and negative Re *vs.* Se correlation for analyses with Re >2500 ppm (–0.59 at minimum significant 0.5, $n = 16$).

Chlorite chemistry and thermometry

Molybdenite is intimately intergrown with chlorite in all the molybdenite-bearing samples studied (Figs 2*f,g*, 3*c,i*, 4*e*, and Supplementary Material – Appendix 3); the only exception is sample Bir-1101/291.2 where chlorite occurs only in the

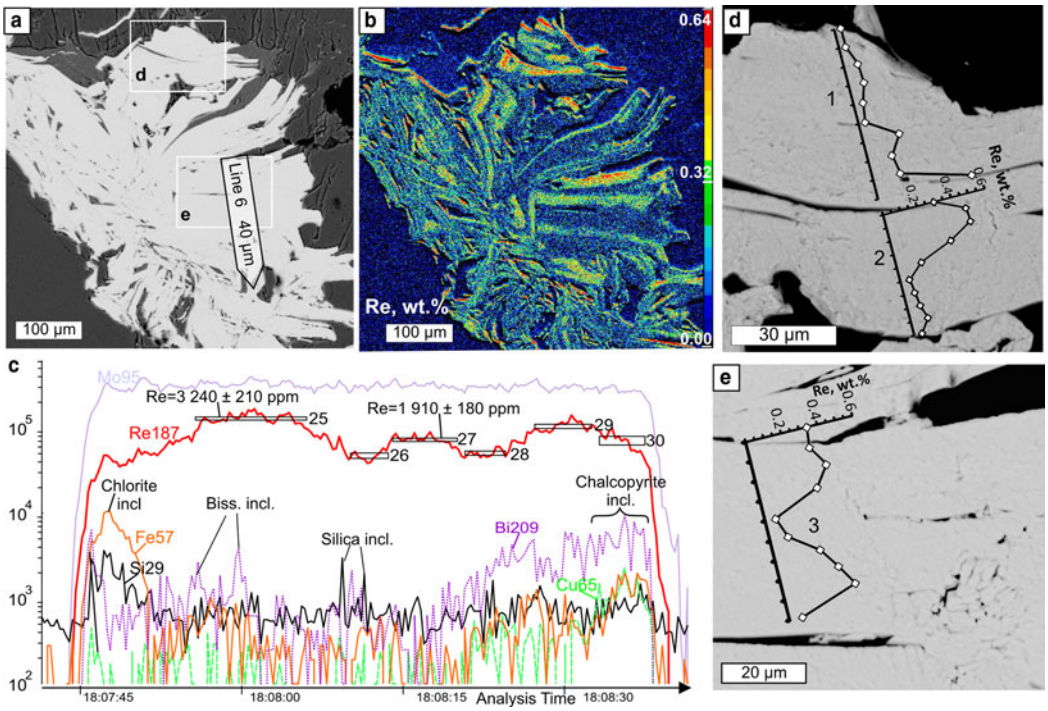

FIG. 7. Molybdenite from Birgilda, sample Bir-1101/237: (*a*) SEM image of a molybdenite 'rosette' showing the position of the LA-ICP-MS profile; (*b*) calibrated map of the Re content (wt.%); (*c*) LA-ICP-MS spectra for line 6; (*d*,*e*) fragments of (*a*) with EMPA profiles.

alteration halo. The chlorite chemical composition was obtained in order to evaluate its formation temperature (Table 7, Appendix 3 and Fig. 9). All the chlorite grains from both Kalinovskoe and Birgilda deposits belong to the clinochlore–daphnite series with minor but variable amounts

TABLE 6. Correlation coefficients for trace elements in molybdenite from the Birgilda site inferred from LA-ICP-MS data: significant* correlation coefficients are highlighted in bold.

	Si	Fe	Cu	Ag	Zn	Pb	Sb	Bi	Se	As	W	Re
Si	1											
Fe	0.16	1										
Cu	0.03	**0.94**	**1**									
Ag	**0.50**	**0.53**	**0.44**	1								
Zn	**0.64**	0.00	–0.15	0.23	1							
Pb	0.16	**0.50**	**0.39**	**0.49**	0.22	1						
Sb	–0.02	**0.42**	**0.37**	**0.43**	–0.23	0.33	1					
Bi	0.21	**0.38**	0.25	**0.50**	0.34	**0.95**	0.18	1				
Se	–0.13	–0.18	–0.22	0.08	–0.09	0.32	–0.02	**0.45**	1			
As	–0.24	–0.02	–0.01	–0.11	**–0.40**	–0.03	0.05	0.03	**0.36**	1		
W	0.19	–0.08	–0.02	–0.07	0.23	–0.22	–0.16	–0.28	**–0.75**	**–0.46**	1	
Re	0.01	–0.23	–0.13	–0.30	0.06	**–0.43**	**–0.39**	**–0.42**	**–0.47**	**–0.38**	**0.55**	1

* Minimum significant correlation was accepted as 0.34 for $n = 36$ for 95% confidence, after Fisher and Yates (1963).

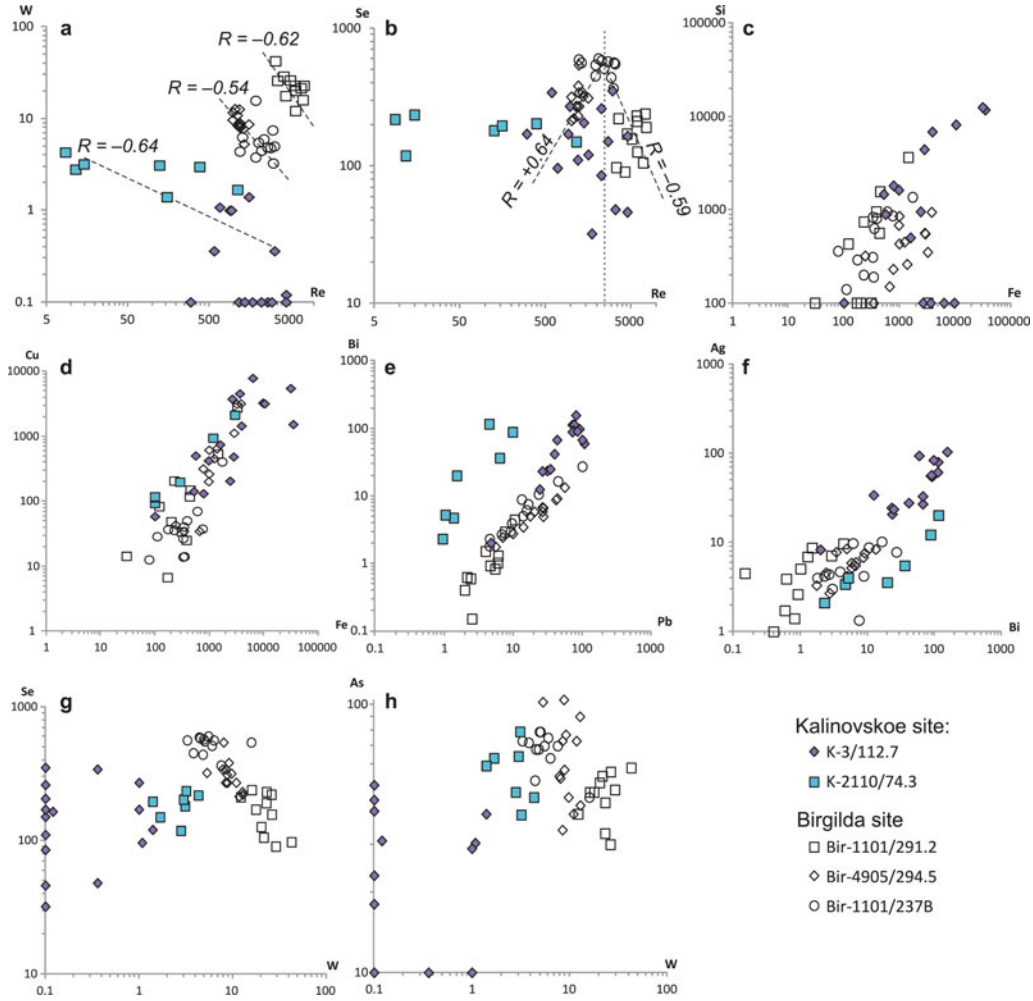

FIG. 8. Binary diagrams for selected trace elements in molybdenite (LA-ICP-MS data).

of amesite (Bailey, 1988); *X*(Mg) varies from 0.38 to 0.72 (Fig. 9). Each sample is characterized by a rather narrow *X*(Mg) range, e.g. 0.38–0.45 in sample K-2210/73.4 (the lowest observed value) and 0.70–0.72 in sample Bir-1101/237 (the highest value). Samples from the Birgilda deposit generally show higher *X*(Mg) values than samples from Kalinovskoe. Almost all chlorite grains contain MnO (up to 0.79 wt.%) but no K_2O, Na_2O and CaO were detected (Table 7 and Appendix 3). Cr_2O_3 (up to 1.49 wt.%) was detected only in sample Bir-1101/291.2 which may be due to the influence of the host basalt. The Si/Al ratio varies from 0.92 (at Kalinovskoe) to 1.16 (at Birgilda). Chlorite-formation temperatures were calculated according to (Cathelineau 1988; Kranidiotis and MacLean, 1987; Kotelnikov *et al*., 2012) and these temperatures all lie between 244 and 368°C (Table 7).

Fluid-inclusion study

Fluid inclusions appropriate for microthermometric studies were found in only four double-polished sections of samples K-2010/73.4 and K-8/100.6 from Kalinovskoe and Bir-1101/237 and Bir-4905/294.5 from Birgilda.

Fluid-inclusion petrography

In both the Kalinovskoe samples, fluid inclusions were observed in euhedral quartz crystals

TABLE 7. Chemical composition of chlorite (wt.%) associated with molybdenite and calculated temperature (°C); see Appendix 3 for the full data.

	K-2210/73.4			K-8/100.6			K-3/112.7			K-1050/157.5			Bir-1101/237			Bir-1101/291.2			Bir-4905/294.5			Bir-42/82		
	$n = 10$			$n = 10$			$n = 10$			$n = 12$			$n = 5$			$n = 8$			$n = 6$			$n = 3$		
Sample	Min	Max	Mean	Min	Max	Mean	Min	Max	Mean	Min	Max	Mean	Min	Max	Mean	Min	Max	Mean	Min	Max	Mean	Min	Max	Mean
SiO_2	23.44	25.42	24.43	23.76	25.58	24.87	25.24	26.12	25.77	26.03	27.48	26.81	25.71	28.20	27.26	26.71	28.53	27.75	25.62	26.42	26.07	26.46	27.06	26.83
Al_2O_3	19.31	21.04	20.40	19.58	22.33	20.95	21.35	22.84	22.13	20.64	23.04	21.55	19.69	21.79	20.87	19.78	20.83	20.37	21.43	23.32	22.63	19.56	20.01	19.77
Cr_2O_3	<dl			<dl			<dl			<dl			<dl			<dl	1.49	1.22	<dl			<dl		
FeO	26.86	29.91	28.69	22.98	25.20	24.05	18.42	19.83	18.96	17.59	22.97	19.43	14.61	15.38	15.06	16.58	17.16	16.98	18.33	19.01	18.56	19.41	19.94	19.73
MnO	<dl	0.46		<dl	0.21		0.06	0.42	0.26	<dl	0.56		0.18	0.34	0.26	0.29	0.38	0.35	0.07	0.32	0.17	0.76	0.79	0.77
MgO	10.00	12.08	10.94	13.33	14.56	13.93	15.93	17.27	16.70	15.58	20.23	18.02	20.30	22.51	21.76	20.78	22.20	21.59	17.94	18.86	18.43	18.18	18.71	18.51
Si*	5.35	5.74	5.50	5.33	5.63	5.50	5.49	5.65	5.55	5.50	5.74	5.62	5.57	5.69	5.62	5.49	5.68	5.59	5.38	5.49	5.44	5.65	5.67	5.66
Al	5.16	5.65	5.41	5.29	5.78	5.46	5.50	5.82	5.62	5.10	5.65	5.32	4.91	5.18	5.07	4.69	4.98	4.84	5.42	5.67	5.57	4.87	4.94	4.91
Cr	–	–	–	–	–	–	–	–	–	–	–	–	–	–	–	–	0.24	0.17	–	–	–	–	–	–
Fe^{3+}	–	–	–	–	–	–	–	–	–	–	–	–	–	–	–	–	–	–	–	–	–	–	–	–
Fe^{2+}	4.98	5.61	5.39	4.18	4.65	4.44	3.34	3.56	3.41	3.07	4.07	3.40	2.53	2.78	2.59	2.79	2.92	2.86	3.17	3.34	3.23	3.47	3.49	3.47
Mn	–	0.09	0.04	–	0.04	0.01	0.01	0.08	0.05	–	0.10	0.03	0.03	0.06	0.05	0.05	0.06	0.06	0.01	0.06	0.03	0.13	0.14	0.14
Mg	3.40	4.00	3.67	4.38	4.75	4.59	5.13	5.51	5.36	4.92	6.20	5.62	6.55	6.78	6.68	6.39	6.57	6.48	5.62	5.81	5.73	5.79	5.84	5.82
Fe_{tot}	4.98	5.61	5.39	4.18	4.65	4.44	3.34	3.56	3.41	3.07	4.07	3.40	2.53	2.78	2.59	2.79	2.92	2.86	3.17	3.34	3.23	3.47	3.49	3.47
$Al^{(IV)}$	2.26	2.65	2.50	2.37	2.67	2.50	2.35	2.51	2.45	2.26	2.50	2.38	2.31	2.43	2.38	2.32	2.51	2.41	2.51	2.62	2.56	2.33	2.35	2.34
$Al^{(VI)}$	2.76	3.02	2.91	2.73	3.23	2.96	3.05	3.44	3.18	2.67	3.23	2.94	2.60	2.75	2.68	2.35	2.62	2.43	2.91	3.05	3.01	2.54	2.59	2.57
Si/Al	0.95	1.11	1.02	0.92	1.06	1.01	0.97	1.02	0.99	0.99	1.12	1.06	1.08	1.16	1.11	1.13	1.21	1.16	0.95	1.01	0.98	1.14	1.16	1.15
X(Mg)	0.38	0.45	0.40	0.49	0.52	0.51	0.60	0.62	0.61	0.54	0.66	0.62	0.70	0.72	0.72	0.68	0.70	0.69	0.63	0.65	0.64	0.62	0.62	0.62
X(Fe)	0.55	0.61	0.59	0.48	0.51	0.49	0.38	0.40	0.39	0.33	0.45	0.38	0.27	0.30	0.28	0.30	0.31	0.30	0.35	0.37	0.36	0.37	0.37	0.37
T_1**	302	365	341	319	368	341	317	342	332	301	341	321	310	330	322	311	343	326	341	360	350	314	317	315
T_2	258	299	283	269	301	283	267	284	277	257	284	270	263	276	271	264	284	273	284	296	289	265	267	266
T_3	301	345	328	304	339	320	297	313	306	284	308	298	283	298	292	286	307	296	311	323	316	294	296	295
T_4	244	279	266	254	281	266	252	266	261	244	266	255	248	259	255	249	267	257	266	277	271	250	252	251

*Formula units are calculated on the basis of 20 cations.

** T_1 after Cathelineau (1988); T_2 and T_3 after Kranidiotis and MacLean (1987) for low-Al and high-Al environments, respectively; T_4 after Kotelnikov *et al*. (2012).

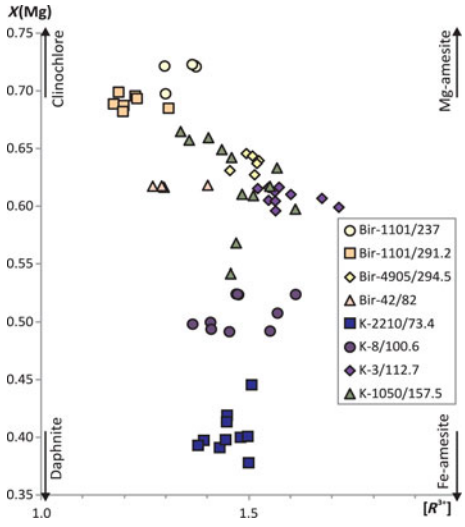

FIG. 9. Compositional variations of chlorite intergrown with molybdenite from Kalinovskoe and Birgilda. [R^{3+}] is the sum of the trivalent cations in the octahedral sites. Classification of chlorites after Bailey (1988).

overgrown by molybdenite (Fig. 10*a*). The quartz is interpreted as preceding the molybdenite formation. At room temperature, two coexisting types of fluid inclusions were identified: (1) VL_1L_2-type fluid inclusions have oval or negative crystal shapes and range from 10 to 15 μm in size; they consist of aqueous liquid and vapour bubbles (30–50 vol.%) surrounded by a thin rim of carbonic liquid (Fig. 10*b*); and (2) V-type inclusions, 10–15 μm in size, consisting of vapour, sometimes with a thin rim of liquid.

In the two samples from Birgilda, fluid inclusions were found in anhedral quartz grains that form intimate intergrowths with molybdenite (Fig. 10*c*) and are cut by carbonate veinlets. The quartz grains are presumed to have formed at the same time as the molybdenite. They contain fluid inclusions of VL-type, which are irregularly shaped, range from 10 to 20 μm in size, and consist of aqueous liquid and a vapour bubble that occupies some 20–30 vol.% of the inclusions (Fig. 10*d*).

All these inclusions are considered to be primary according to the criteria proposed by Roedder (1984). No daughter minerals or trapped solids were observed.

Microthermometry of fluid inclusions

The results of a microthermometric study are presented in Table 8 and Fig. 11.

Fluid inclusions of the VL_1L_2 type from Kalinovskoe show low salinities (10.4 to 12 wt.% NaCl equiv.) and eutectic temperatures of –43 to –39°C indicating that divalent chlorides (Mg^{2+} and (or) Fe^{2+}) are dominant. The VL_1L_2 and V types of inclusion both have $T_m(CO_2)$ from –58.5 to −58.9°C which is lower than for pure CO_2 (–56.6° C), suggesting a small admixture of CH_4 (Collins, 1979). VL_1L_2-type inclusions homogenize to the liquid phase upon heating at 365 to 502°C. Pressure, as calculated for single-phase CO_2-bearing inclusions from Kalinovskoe, corresponds to 650–802 bar. These data are in agreement with previous results for Kalinovskoe (Groznova *et al.*, 2015).

Fluid inclusions of the VL type from Birgilda show moderate salinities (12.7–18.9 wt.% NaCl equiv.) and eutectic temperatures of –38.5 to –30°C indicating the presence of both NaCl and divalent chlorides. They homogenize to the liquid phase at 195–265°C.

The coexistence among the VL_1L_2 and V types of fluid inclusion in the Kalinovskoe samples suggests that the fluids had undergone CO_2 effervescence. In this case the estimates of T_h can be regarded as real trapping temperatures (Roedder, 1984). For VL-type inclusions from Birgilda the T_h estimates may be considered as minimum trapping temperatures. It is worth noting that the T_h estimates for sample Bir-1101/237 (230–265, mean 248°C) overlap with the temperature estimates obtained for chlorite (248–259, mean 255°C, Table 7) calculated after Kotelnikov *et al.* (2012). The T_h estimates for sample Bir-4905/294.5 (195–221, mean 208°C) are somewhat lower than the temperatures obtained from chlorite geothermometry (249–267, mean 257°C, Table 7). There is no reliable pressure estimate for the Birgilda samples but the pressure was probably similar to that estimated for late-stage mineralization at Kalinovskoe and in the range 190–350 bars (Groznova *et al.*, 2015). Pressure corrections for the homogenization temperatures (Potter, 1977) will, in this case, increase the temperature estimate by 30°C, to 225–351°C. If the pressure is higher and ~760 bar as suggested for the early Kalinovskoe assemblages, then the correction will reach 70°C (265–271°C). Both intervals overlap with the temperatures calculated from chlorite geothermometry (Kotelnikov *et al.*, 2012).

Discussion

Re-Os dating of molybdenite

Previous Re-Os dating of three molybdenite samples from the marginal zone at Kalinovskoe

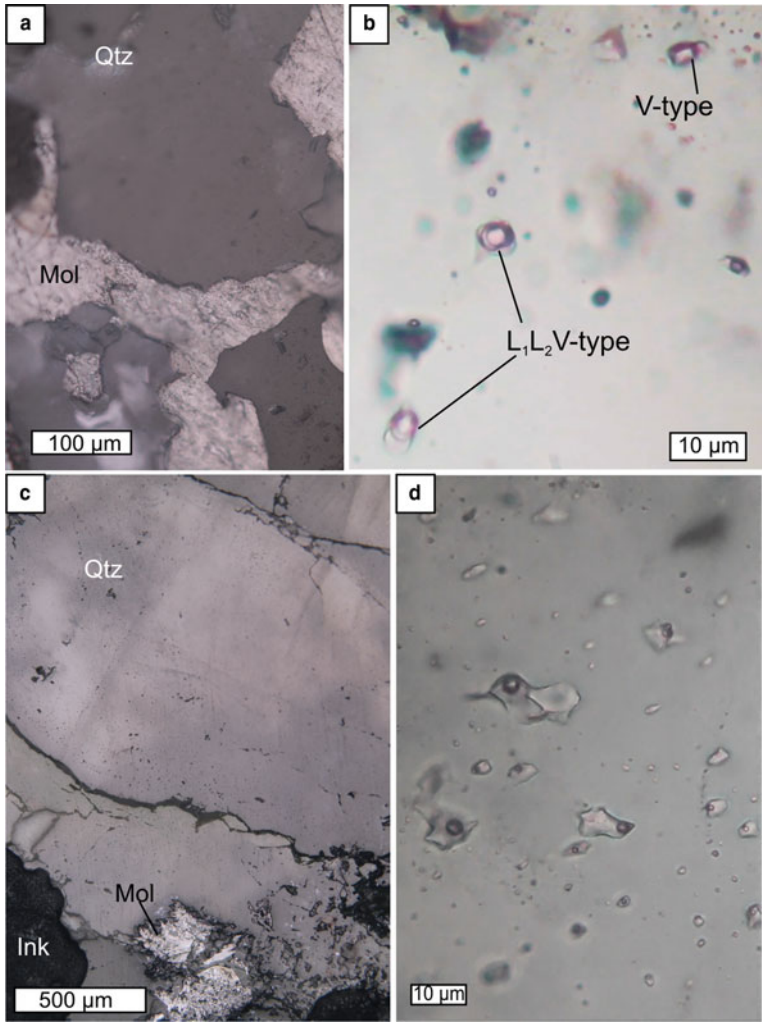

FIG. 10. Two types of fluid inclusions measured at the Kalinovskoe (*a*,*b*) and Birgilda (*c*,*d*) sites. (*a*) quartz overgrown by molybdenite, reflected light, sample K-2010/73.4; (*b*) enlarged fragment of (*a*) in transmitted light, inclusions of VL_1L_2- and V-types; (*c*) quartz intergrown with a molybdenite rosette, reflected light, sample Bir-4905/294.5; (*d*) enlarged fragment of (*c*) in transmitted light, inclusions of VL type.

(Tessalina and Plotinskaya, 2017) gave ages of 427.1 ± 3.3 Ma to 431.7 ± 1.7 Ma; the latter result relates to the low-Re molybdenite (sample K-2110/74.3) described in the present study. The age obtained during the present study using the high-Re molybdenite sample (K-3/112.7) from the central part of the Kalinovskoe deposit (431.9 ± 1.9 Ma) agrees well with the previous data. The age obtained for the high-Re molybdenite from the Birgilda deposit (432.0 ± 1.7 Ma) is similar. The two ages presented here and those from the earlier work can be considered to represent a single age population, within the analytical uncertainty, that concurs with the emplacement age of the ore-bearing porphyry diorite stock at Tomino (428 ± 3 Ma) obtained by zircon dating (Grabezhev *et al*., 2013).

Trace elements in molybdenite

The trace-element contents of molybdenite from Kalinovskoe and Birgilda are generally similar (Tables 3, 4). Molybdenite from Kalinovskoe is slightly higher in Ag and Bi but lower in W and it

TABLE 8. Microthermometric data for primary fluid inclusions in quartz from molybdenite-bearing samples from the Kalinovskoe and Birgilda sites.

Sample	*n*	Incl. type	T_h (°C)	T_e (°C)	$T_{m\ (CO2)}$ (°C)	$T_{h\ (CO2)}$ (°C)	$T_{m\ (clath)}$ (°C)	$T_{m\ (ice)}$ (°C)	C (wt.% NaCl equiv)	Pressure (bar)	Density (g/cm^3)
K-8/ 100.6	12	VL_1L_2	365 to 465 (440)*	−42.9 to −38.7 (−41.4)	−58.8 to −58.5 (−58.6)	21 to 32.5 (28.5)	3.1 to 4.0 (3.5)	n.d.	10.5 to 11.7 (11.2)	760	0.5 to 0.6
	8	V	n.d.	n.d.	−58.8	25.1 to 30 (29.6)	n.d.	–	–	n.d.	n.d.
<dl	7	VL_1L_2	374 to 502 (431)	−42.3 to −39.0 (−40.1)	−58.9 to −58.5 (−58.6)	18 to 30 (22.4)	2.8 to 3.8 (3.3)	–	10.4 to 12 (11.4)	650 to 802 (758)	0.5 to 0.6
<dl	9	V	n.d.	n.d.	−58.9 to −58.8 (−58.7)	26.1 to 31.1 (28.3)	n.d.	–	–	n.d.	n.d.
Bir-1101/ 237	8	VL	230 to 265 (248)	−38.5 to −36.5 (−37.4)	n.d.	n.d.	–	−15 to −13.8 (−14.5)	17.6 to 18.9 (18.2)	–	–
Bir-4905/ 294.5	10	VL	195 to 221 (208)	−34.1 to −30.0 (−32.3)	–	–	–	−10.2 to −8.9 (−9.6)	12.7 to 14.2 (13.5)	–	–

Notes: T_h – total homogenization temperature, T_e – eutectic temperature, $T_{m(CO2)}$ – CO_2 melting temperature; $T_{h\ (CO2)}$ – CO_2 homogenization temperature, $T_{m\ (clath)}$ – clathrate melting temperature, $T_{m\ (ice)}$ – final ice melting temperature, C– salinity.
* – average value.

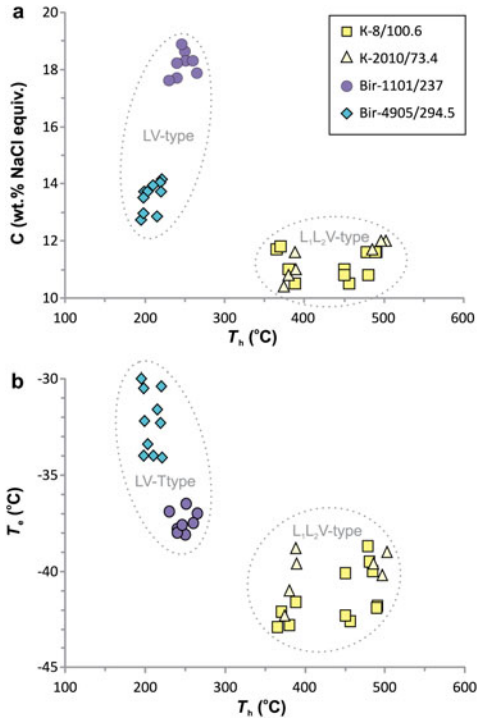

FIG. 11. Homogenization temperatures *vs*. salinity (*a*) and homogenization temperature *vs*. eutectic temperatures (*b*) for individual fluid inclusions.

also shows a wider range of Re content than that from Birgilda. Overall, the Re content of both sites is similar to molybdenite from the Tomino deposit, where Grabezhev and Hiller (2015) reported 0.04 to 0.38 wt.% Re by EMPA point analyses and 0.05 to 0.26 wt.% by ICP-MS analyses of molybdenite mineral fractions. This is also similar to calculated Re contents from spectrophotometry analysis of bulk samples which gave values of 440–3140 ppm Re in molybdenite (Grabezhev, 2013).

Correlation analysis revealed a group of elements with positive correlations: Si, Fe, Co, Cu, Zn, Ag, Sb, Te, Pb and Bi. For Kalinovskoe this group includes Au, while As and Se are included at Birgilda. Mineralogical data provide evidence that all these elements form mineral inclusions in molybdenite. Numerous discrete regions within the LA-ICP-MS profiles indicating elevated proportions of these elements (Figs 4*h*,*i*,*k*, 5*g*, 6*c*, 7*c*) support this conclusion. The Si–Fe correlation, most evident in sample K-3/112.7 (Fig. 8*c*), is likely to be the result of multiple intergrowths of molybdenite with chlorite and, to a lesser degree, with epidote (Figs 2*b*,*f*, 3*c*,*f*,*h*,*i*, 4*e*). Numerous inclusions of chalcopyrite (Figs 3*e*, 4*j*, 5*c*) resulted in positive Fe–Cu correlations (Fig. 8*d*). Inclusions of matildite (Fig. 2*h*), and, perhaps, of other Bi- and Pb-sulfosalts and tellurides led to positive correlations for Pb–Bi, Bi–Ag (Fig. 8*e*,*f*), Bi–Cu and Bi–Te.

Rhenium, which has either no correlation or a negative correlation with the other trace elements (using LA-ICP-MS data) also shows a negative correlation with Mo in the EMPA analyses and is most likely to be incorporated in the molybdenite lattice. Inclusions of rheniite, similar to those described by Voudouris *et al*. (2009) and too small to be detectable by SEM cannot, however, be ruled out. Other elements including W and Se can be incorporated into the molybdenite structure with Re (see review in Pašava *et al*., 2016 for detailed references). However, W demonstrates extremely irregular LA-ICP-MS spectra (Figs 4–6) suggesting the presence of inclusions of W-bearing minerals. High Se contents (1000 ppm or more) bound isomorphically to molybdenite were proven by Ciobanu *et al*. (2013) based on an LA-ICP-MS study. Moreover, Kalinin *et al.* (2013) reported up to 15 wt.% of Se in molybdenite based on EMPA data. In the Birgilda deposit, positive Re *vs*. Se correlation for analyses with <2500 ppm Re suggests that some Se may be incorporated in the molybdenite lattice. However, our previous mineralogical study of the Kalinovskoe ore (Plotinskaya *et al*., 2014b) revealed up to 0.69 wt.% Se in matildite and 0.57 wt.% Se in tetradymite which, in addition to a positive Se–Bi correlation (Table 5), provides evidence that Se is mainly due to mineral inclusions in molybdenite.

Deposit-scale variations of rhenium

The limited number of samples investigated does not allow any conclusions to be drawn on variations of the Re content of molybdenite on a deposit scale. Most samples from Kalinovskoe and Birgilda have high Re contents averaging 1200 to 5700 ppm (Table 4). No correlation with the host rocks is evident; diorite- and basalt-hosted samples have similar molybdenite Re contents. The only exception is sample K-2210/73.4 with Re contents considerably lower than the other samples and averaging 71 ppm. This value is close to two other samples from the same ore body (drill hole K-2210) reported by Tessalina and Plotinskaya (2017) with Re contents of 147 and 228 ppm Re. Perhaps this is a feature of this peripheral ore body, but that requires further investigation.

Rhenium distribution in individual grains of molybdenite

All the samples investigated demonstrate extremely irregular Re distributions in single molybdenite flakes. The Re contents vary by one or two orders of magnitude, *e.g.* from 302 to 4540 ppm in sample K-3/112.7, or from <10 to >1000 ppm in sample K-2210/73.4 (Table 4). The irregular distribution of Re in molybdenites from deposits of various genetic types has been identified by EMPA (Kovalenker *et al*., 1974; Voudouris *et al*., 2009; Maksimyuk and Kulikova, 2013; Rathkopf *et al*., 2017), by LA-ICP-MS (Ciobanu *et al*., 2013; Bogdanov and Krumov, 2016; Kovalenker *et al*., 2018, *etc.*), and by NanoSIMS (Barra *et al.*, 2017). Aleinikoff *et al.* (2012) and Ciobanu *et al.* (2013) also noted variations in W and Se. This suggests that the irregular distribution of rhenium in single grains of molybdenite is a common phenomenon.

X-ray mapping using the Re$L\alpha$ line (Figs 4*b*,*d*,*f*, 5*b*,*f*, 6*b*, 7*b*) showed that most Re-enriched areas form linear zones up to tens of μm wide. Similar linear distribution patterns were revealed in molybdenites from other porphyry Cu-(Mo) deposits of the Urals by X-ray mapping, such as the Verkhneuralskoe Mo-porphyry occurrence (Grabezhev *et al*., 2013; Plotinskaya *et al*., 2014a), the Voznesenskoe Cu-porphyry deposit (Grabezhev and Voudoris, 2014) and the Mikheevskoe Cu-porphyry deposit (Grabezhev and Shagalov, 2010; Plotinskaya *et al*., 2015). Perhaps there are Re-enriched layers, or groups of layers, within the molybdenite structure. It has been assumed that such layers could be formed of the 3R-polytypes of molybdenite (*e.g.* Newberry, 1979; Rekharskii *et al*., 1983; Filimonova *et al*., 1984; Melfos *et al*., 1991; Maksimyuk and Kulikova, 2013). However, the presence of high Re contents in both natural (Voudouris *et al*., 2009; Ciobanu *et al*., 2013) and synthetic (Drabek *et al*., 2010) molybdenites formed of the 2H-polytype suggests other mechanisms of incorporation of Re into the molybdenite structure. For example, Ciobanu *et al.* (2013) attributed a high Re content to lattice defects in 2H-molybdenite.

Controls of Re incorporation in molybdenite

The controls of Re incorporation in molybdenite have been discussed by Berzina *et al*. (2005) and in experimental studies by Xiong *et al*. (2006). It has been established that lower temperatures and a decrease in f_{O_2} are favourable for the formation of high-Re molybdenite. Both the high- and low-Re molybdenite observed in this study have similar

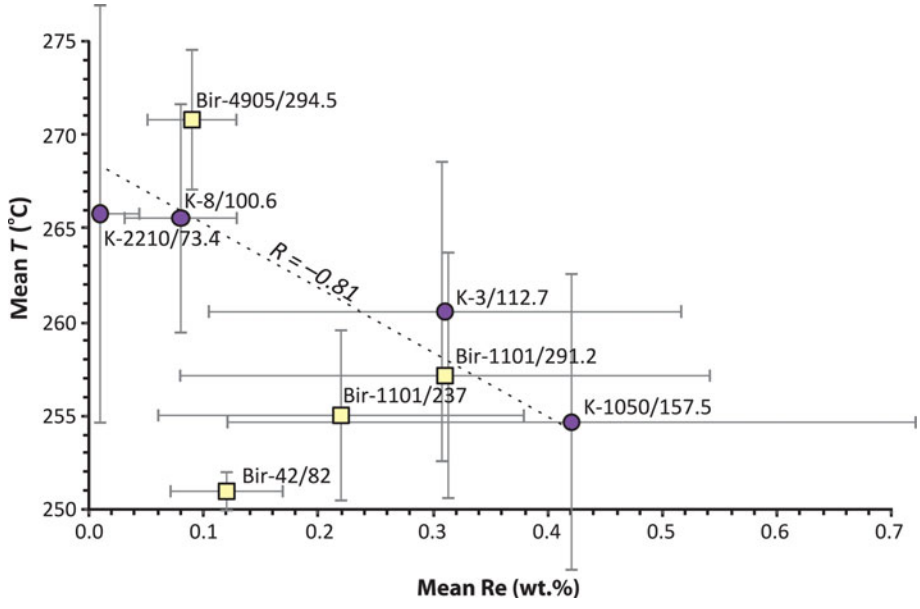

FIG. 12. Mean *T* (°C) *vs*. mean wt.% Re from the EPMA analyses (Table 3). Error bars are shown for 1 sd. The temperature was calculated after Kotelnikov *et al*. (2012) (Table 2). The correlation coefficient is given for the whole dataset excluding sample Bir-42/82.

assemblages (chalcopyrite, pyrite, chlorite, epidote, muscovite, calcite) which does not allow any estimation of differences in variation of f_{O_2}. Chlorite, however, can be used to test the temperature influence on the incorporation of Re in molybdenite. The chlorite thermometer of Kotelnikov *et al*. (2012) was selected because it gives a better agreement with the fluid-inclusion results from the two Birgilda samples. Figure 12 shows mean the Re contents *vs*. mean calculated temperatures. Samples with higher Re contents (K-1050/157.5, K-3/112.4, Bir-1101/291.2 and Bir-1101/237) were formed at lower temperatures than those with lower Re contents (K-2210/73.4, K-8/100.6, and Bir-4905/294.5). Sample Bir-42/84 is the only exception, but the temperature was calculated from only three chlorite analyses and, thus, may be unrepresentative. The remaining seven samples demonstrate a significant negative correlation (–0.81) between temperature and Re content.

Sources of rhenium and other metals

It has been suggested that high Re contents in molybdenite provide evidence for a mantle input (Stein *et al*., 2001; Sun *et al.,* 2004, *etc.*). Reviews by Mao *et al*. (2013) and Pašava *et al.* (2016), using data from the literature, propose that <10 ppm Re in molybdenite indicates crustal sources, 10–100 ppm indicates a mixed mantle/crustal source and >100 ppm Re in molybdenite indicates molybdenite derived from mantle sources. Therefore, the high Re contents of most molybdenites from Kalinovskoe and Birgilda may indicate a predominantly mantle source for the metals. The Sm-Nd systematics of the diorite porphyry intrusions of the Birgilda-Tomino igneous complex (Grabezhev, 2009) confirms a mantle-derived source of the magma and most of the metals. A lead isotope study (Plotinskaya *et al*., 2017*a*) also provided evidence for a mantle-derived lead source. There was, however, the possibility of some input of both magma and metals from a crustal source such as might have been produced in a mature volcanic arc with the input of sediments containing crustal lead from denudation of pre-Cambrian crust into a subduction zone. This could explain the deposit-scale variation of Re content in molybdenite observed at the Kalinovskoe deposit.

Conclusions

The trace-element patterns of molybdenite from the Kalinovskoe and Birgilda porphyry copper deposits of the Urals are broadly similar. Most trace elements (Si, Fe, Co, Cu, Zn, Ag, Sb, Te, Pb, Bi, Au, As and Se) form mineral inclusions within molybdenite. Rhenium is most likely to be incorporated into the molybdenite lattice.

The present results demonstrate an extremely irregular distribution of Re within individual molybdenite flakes, with Re-enriched areas forming μm-scale linear zones. A negative relationship is shown between the Re contents of molybdenite and the temperature of formation of the co-existing chlorite.

The high Re contents (up to 1.13 wt.%) in molybdenite indicate a mantle-derived source.

Acknowledgements

This study was supported by the NHM, London (*via* the CERCAMS Fellowship Program), by the Presidium of the Russian Academy of Sciences (Program No. 48), and, partly, by the Russian Foundation for Basic Research, Project No 16-05-00622. RS acknowledges funding under NERC Grant NE/P017452/1 "From arc magmas to ores (FAMOS): A mineral systems approach".

The authors thank the staff of the Russian Copper Company for assistance during the fieldwork. A.I. Grabezhev is acknowledged for providing a sample from the Birgilda deposit (Bir-42/84). A. Kearsly and T. Salge (NHM) are acknowledged for their assistance with the SEM/EDS analysis. The manuscript benefited from extensive reviews by two anonymous reviewers. Editorial assistance from K. Sundblad and J. Bowles is much appreciated.

Supplementary material

To view supplementary material for this article, please visit https://doi.org/10.1180/minmag.2017.081.106

References

Aleinikoff, J.N., Creaser, R.A., Lowers, H.A., Magee, C. W. and Grauch, R.I. (2012) Multiple age components in individual molybdenite grains. *Chemical Geology*, **300–301**, 55–60.

Bailey, S.W. (1988) Chlorites: structures and crystal chemistry. Pp. 347–403 in: *Hydrous Phyllosilicates (Exclusive of Micas)* (S.W. Bailey, editor). Reviews in Mineralogy, **19**. Mineralogical Society of America, Washington, D.C.

Barra, F., Deditius, A., Reich, M., Kilburn, M.R., Guagliardo, P. and Roberts, M.P. (2017) Dissecting

the Re-Os molybdenite geochronometer. *Scientific Reports*, **7**, 16054. https://doi.org/10.1038/s41598-017-16380-8

Berzina, A.N., Sotnikov, V.L., Economou-Eliopoulos, M. and Eliopoulos, D.C. (2005) Distribution of rhenium in molybdenite from porphyry Cu–Mo and Mo–Cu deposits of Russia (Siberia) and Mongolia. *Ore Geology Reviews*, **26**, 91–113.

Bodnar, R.J. and Vityk, M.O. (1994) Interpretation of microthermometric data for H_2O–NaCl fluid inclusions. Pp. 117–130 in: *Fluid Inclusions in Minerals, Methods and Applications* (B. De Vivo and M.L. Frezzotti, editors). Virginia Tech, Blacksburg, Virginia, USA.

Bogdanov, K. and Krumov, I. (2016) Trace element vectors in molybdenite from porphyry-copper deposits of Bulgaria. Pp. 17–18 in: *Bulgarian Geological Society, National Conference with International Participation GEOSCIENCES 2016*.

Brown, P. (1989) FLINCOR: a computer program for the reduction and investigation of fluid inclusion data. *American Mineralogist*, **74**, 1390–1393.

Cathelineau, M. (1988) Cation site occupancy in chlorite and illites as a function of temperature. *Clay Minerals*, **23**, 471–485.

Ciobanu, C.L., Cook, N.J., Kelson, C.R., Guerin, R., Kalleske, N. and Danyushevsky, L. (2013) Trace element heterogeneity in molybdenite fingerprints stages of mineralization. *Chemical Geology*, **347**, 175–189.

Collins, P.L.F. (1979) Gas hydrates in CO_2-bearing fluid inclusions and the use of freezing data for estimation of salinity. *Economic Geology*, **74**, 1435–1444.

Crawford, M.L. (1981) Phase equilibria in aqueous fluid inclusions. Pp. 75–100 in: *Fluid Inclusions: Applications to Petrology* (L.S. Hollister and M.L. Crawford, editors). Mineralogical Association of Canada Short Course Handbook, **6**. Mineralogical Association of Canada, Quebec, Canada.

Dill, H.G. (2010) The "chessboard" classification scheme of mineral deposits: mineralogy and geology from aluminum to zirconium. *Earth Science Reviews*, **100**, 1–420.

Drabek, M., Rieder, M. and Bohmova, V. (2010) The Re–Mo–S system: new data on phase relations between 400 and 1200°C. *European Journal of Mineralogy*, **22**, 479–484.

Filimonova, L.E., Zhukov, N.M. and Malyavskaya, A.T. (1984) The genetic aspects of polytypes and content of Re in molybdenite at the porphyry copper deposits. *Geokhimiya*, 1040–1046 [in Russian].

Fisher, R.A. and Yates, F. (1963) *Statistical Tables for Biological, Agricultural and Medical Research*, 6th Edition, Oliver & Boyd, Edinburgh and London.

Grabezhev, A.I. (2009) Sr–Nd–C–O–H–S isotope-geochemical description of South Urals porphyry-copper fluid-magmatic systems: probable sources of matter. *Lithosphera*, **6**, 66–89 [in Russian with English abstract].

Grabezhev, A.I. (2013) Rhenium in porphyry copper deposits of the Urals. *Geology of Ore Deposits*, **55**, 13–26.

Grabezhev, A.I. and Belgorodskii, E.A. (1992) *Ore-Bearing Granitoids and Metasomatites of Copper Porphyry Deposits*. Nauka, Yekaterinburg, Russia [in Russian].

Grabezhev, A.I. and Gmyra, V.G. (2014) Rhenium distribution in deformed molybdenite: evidence from the data of microprobe scanning (Voznesenskoe porphyry copper deposit, South Urals, Russia). *Doklady Earth Sciences*, **454**, 175–178.

Grabezhev, A.I. and Hiller, V.V. (2015) Rhenium in molybdenite of Tominsk Porphyry Copper Deposit (the South Urals): Results of the microprobe study. Pp. 81–93 in: *Proceedings of the Russian Mineralogical Society, CXLIV* [in Russian with English abstract].

Grabezhev, A.I. and Shagalov, E.S. (2010) Rhenium distribution in molybdenite: results of microprobe scanning (porphyry copper deposits, the Urals). *Doklady Earth Sciences*, **431**, 351–355.

Grabezhev, A.I. and Voudouris, P.C. (2015) Rhenium distribution in molybdenite from the Vosnesensk porphyry Cu ± (Mo,Au) deposit (Southern Urals, Russia). *The Canadian Mineralogist*, **52**, 671–686.

Grabezhev, A.I., Kuznetsov, N.S. and Puzhakov, B.A. (1998) *Ore and alteration zoning of sodium type copper-porphyry column (paragonite-bearing aureoles, the Urals)*. IGG Publishing House, Yekaterinburg, Russia [in Russian].

Grabezhev, A.I., Sazonov, V.N., Murzin, V.V., Moloshag, V.P., Sotnikov, V.I., Kuznetsov, N.S., Pyzhakov, B.A. and Pokrovsky, B.G. (2000) The Bereznyakovsk gold deposit (South Urals, Russia). *Geology of Ore Deposits*, **42**, 33–46.

Grabezhev, A.I., Bea, F., Montero, M.P. and Fershtater, G. B. (2013) The U-Pb SHRIMP age of zircons from diorites of the Tomino–Bereznyaki ore field (South Urals, Russia): evolution of porphyry Cu-epithermal Au-Ag system. *Russian Geology and Geophysics*, **54**, 1332–1339.

Groznova, E.O., Plotinskaya, O.Y., Abramov, S.S., Borovikov, A.A., Milovska, S., Luptakova, J. and Seltmann, R. (2015) Porphyry and epithermal deposits of the Urals: *PTx*-parameters. Pp. 70–71 in: *European Current Research on Fluid Inclusions (ECROFI-XXIII)*. School of Earth and Environment, University of Leeds, UK.

Kalinin, A.A., Savchenko, Y.E. and Selivanova, E.A. (2013) Rhenium- and selenium-bearing molybdenite in Ozernoye ore occurrence in Salla-Kuolajarvinskaya zone, northern Karelia. *Proceedings of the Russian Mineralogical Society*, **142**, 104–114 [in Russian with English abstract].

Kallistov, G.A. (2014) Duration and stages of emplacement of the Chelyabinsk granitoid batholith. *IGG UrB RAS Yearbook-2013*, **161**, 343–349 [in Russian].

Kaluzhny, V.A. (1982) *Principles of Theory of Mineral-Forming Fluids*. Naukova Dumka, Kiev [in Russian].

Kotelnikov, A.R., Suk, N.I., Kotelnikova, Z.A., Tschekina, T.I. and Kalinin, G.M. (2012) Mineral geothermometers for low-temperature paragenesis. *Vestnik Otdelenia nauk o Zemle*, **4**, NZ9001. https://doi.org/10.2205/2012NZ_ASEMPG.

Kovalenker, V.A., Laputina, I.P. and Vyalsov, L.N. (1974) On rhenium-rich molybdenite from the Talnakh copper–nickel deposit, Norilsk district. *Doklady AN SSSR*, **217**, 187–189 [in Russian].

Kovalenker, V.A., Trubkin, N.V., Abramova, V.D., Plotinskaya, O.Y., Kiseleva, G.D., Borisovskii, S.E. and Yazykova, Y.I. (2018) Typomorphic characteristics of molybdenite from the Bystrinskoe Cu-Au skarn-porphyry deposit, Eastern Transbaikalia, Russia. *Geology of Ore Deposits*, **60**. https://doi.org/10.1134/S107570151801004X

Kranidiotis, P. and MacLean, W.H. (1987) Systematics of chlorite alteration at the Phelps Dodge massive sulfide deposits, Matagami Quebec. *Economic Geology*, **82**, 1898–1911.

Maksimyuk, I.E. and Kulikova, I.M. (2013) Species of rhenium in molybdenite from various type ore deposits. *Proceedings of the Russian Mineralogical Society*, **142**, 94–106 [in Russian with English abstract].

Mao, Z., Cheng, Y., Liu, J., Yuan, S., Wu, S., Xiang, X. and Luo, X. (2013) Geology and molybdenite Re-Os age of the Dahutang granite-related veinlets-disseminated tungsten ore field in the Jiangxin Province, China. *Ore Geology Reviews*, **53**, 422–433.

Markey, R.J., Hannah, J.L., Morgan, J.W. and Stein, H.J. (2003) A double spike for osmium analysis of highly radiogenic samples. *Chemical Geology*, **200**, 395–406.

Melfos, V., Vavelidis, M., Filippidis, A., Christofides, G. and Evangelou, E. (1991) Re-rich and Re-poor molybdenite in the Maronia rhyolitic intrusion, northeastern Greece. Pp. 775–777 in: *Source, Transport and Deposition of Metals* (M. Pagel and J. Leroy, editors). Balkema, Rotterdam.

Narykova, I.O., Kurchevskaya, E.M. and Yakhno, M.V. (2015) Metasomatites of Birgildinskoye porphyry copper deposit (the Southern Urals). *Proceedings of Siberian Department of the Section of Earth Sciences Russian Academy of Natural Sciences. Geology, Prospecting and Exploration of Ore Deposits*, **52**, 24–35 [in Russian with English abstract].

Newberry, R.J.J. (1979) Polytypism in molybdenite (I): a nonequilibriun impurity induced phenomenon. *American Mineralogist*, **64**, 758–767.

Pašava, J., Svojtka, M., Veselovský, F., Ďurišová, J., Ackerman, L., Pour, O., Drábek, M., Halodová, P. and Haluzová, E. (2016) Laser ablation ICPMS study of trace element chemistry in molybdenite coupled with scanning electron microscopy (SEM) – An important tool for identification of different types of mineralization. *Ore Geology Reviews*, **72**, 874–895.

Paton, C., Hellstrom, J.C., Paul, B., Woodhead, J.D. and Hergt, J.M. (2011) Iolite: Freeware for the visualisation and processing of mass spectrometric data. *Journal of Analytical Atomic Spectrometry*, **26**, 2508–2518.

Plotinskaya, O.Y., Grabezhev, A.I. and Seltmann, R. (2014*a*) Porphyry deposits of the South Urals: rhenium distribution. *Acta Geologica Sinica (English Edition)*, **88**, 584–586.

Plotinskaya, O.Y., Grabezhev, A.I., Groznova, E.O., Seltmann, R. and Lehmann, B. (2014*b*) The Late Paleozoic porphyry-epithermal spectrum of the Birgilda–Tomino ore cluster in the South Urals, Russia. *Journal of Asian Earth Sciences*, **79**, 910–931.

Plotinskaya, O.Y., Grabezhev, A.I. and Seltmann, R. (2015) Rhenium in ores of the Mikheevskoe Mo-Cu porphyry deposit, South Urals. *Geology of Ore Deposits*, **57**, 118–132.

Plotinskaya, O.Y., Chugaev, A.V. and Seltmann, R. (2017*a*) Lead isotope systematics of porphyry-epithermal spectrum of the Birgilda-Tomino ore cluster in the South Urals, Russia. *Ore Geology Reviews*, **85**, 204–215.

Plotinskaya, O.Y., Grabezhev, A.I., Tessalina, S., Seltmann, R., Groznova, E.O. and Abramov, S.S. (2017*b*) Porphyry deposits of the Urals: geological framework and metallogeny. *Ore Geology Reviews*, **85**, 153–173.

Potter, II, R.W. (1977) Pressure corrections for fluid-inclusion homogenization temperatures based on the volumetric properties of the system NaCl–H_2O. *Journal of Research of the U.S. Geological Survey*, **5**, 603–607.

Pravda (2015) http://pravdaurfo.ru/articles/114468-rmk-zapretili-dobyvat-med-v-chelyabinskoy-oblasti, accessed 15.04.2017.

Puchkov, V.N. (2017) General features relating to the occurrence of mineral deposits in the Urals: What, where, when and why. *Ore Geology Reviews*, **85**, 4–29.

Puzhakov, B.A. (1999) Productive granitoids, metasomatism, and mineralization of the Birgil'da–Tomino ore cluster, *Cand. Sci. (Geol.–Mineral.) Thesis*, Yekaterinburg [in Russian].

Rathkopf, C., Mazdab, F., Barton, I. and Barton, M.D. (2017) Grain-scale and deposit-scale heterogeneity of Re distribution in molybdenite at the Bagdad porphyry Cu-Mo deposit, Arizona. *Journal of Geochemical Exploration*, **178**, 45–54.

Rekharskii, V.I., Savel'eva, L.V. and Lange, E.K. (1983) Behaviour of rhenium in ore-forming process. *Izvestia*

Akademii Nauk SSSR, Seria Geologicheskaya, 1040–1046 [in Russian].

Roedder, E. (1984) *Fluid inclusions*. Reviews in Mineralogy, **Vol. 12**, Mineralogical Society of America, Washington, D.C., 646 pp.

Romashova, L.N. (1984) The Birgildinskoe porphyry copper deposit. *Geology of Ore Deposits*, **26**, 20–31 [in Russian].

Samygin, S.G. and Burtman, V.S. (2009) Tectonics of the Ural Paleozoides in comparison with the Tien Shan. *Geotectonics*, **43**, 133–151.

Stein, H.J., Markey, R.J., Morgan, J.W., Hannah, J.L. and Schersten, A. (2001) The remarkable Re ± Os chronometer in molybdenite: how and why it works. *Terra Nova*, **13**, 479–486.

Sun, W., Bennett, V.C. and Kamenetsky, V.S. (2004) The mechanism of Re enrichment in arc magmas: evidence from Lau-Basin basaltic glasses and primitive melt inclusions. *Earth and Planetary Science Letters*, **222**, 101–114.

Sylvester, P.J., Cabri, L.J., Tubrett, M.N., McMahon, G., Laflamme, J.H.G. and Peregoedova, A. (2005) *Synthesis and evaluation of a fused pyrrhotite standard reference material for platinum group element and gold analysis by laser ablation-ICPMS*. Pp. 16–20 in: *Abstract, 10th International Platinum Symposium*.

Tessalina, S. and Plotinskaya, O.Y. (2017) Silurian to Carboniferous Re-Os molybdenite ages of the Kalinovskoe, Mikheevskoe and Talitsa Cu- and Mo porphyry deposits in the Urals: implications for geodynamic setting. *Ore Geology Reviews*, **85**, 174–180.

Thiery, R., Van den Kerkhof, A.M. and Dubessey, J. (1994) VX properties of CH_4–CO_2 and CO_2–N_2 fluid inclusions: modelling for T<31°C and *P*<400 bars. *European Journal of Mineralogy*, **6**, 753–771.

Trach, G.N. and Beskin, S.M. (2011) Resources of rhenium in Russia. *Razvedka i Okhrana Nedr*, 26–31 [in Russian].

Volchkov, A.G., Kuznetsov, V.V. and Nikeshin, Y.V. (2015) Tasks and targets of the national budget funded geological exploration for base metals (Cu, Pb, Zn). *Rudy i Metally*, 30–35 [Russian with English abstract].

Voudouris, P.C., Melfos, V., Spry, P.G., Bindi, L., Kartal, T., Arikas, K., Moritz, R. and Ortelli, M. (2009) Rhenium-rich molybdenite and rheniite in the Pagoni Rachi Mo-Cu-Te-Ag-Au prospect, northern Greece: Implications for the Re geochemistry of porphyry style Cu-Mo and Mo mineralization. *The Canadian Mineralogist*, **47**, 1013–1036.

Wohlgemuth-Ueberwasser, C.C., Ballhaus, C., Berndt, J., Stotter née Paliulionyte, V. and Meisel, T. (2007) Synthesis of PGE sulfide standards for laser ablation inductively coupled plasma mass spectrometry (LA-ICP-MS). *Contributions to Mineralogy and Petrology*, **154**, 607–617.

Xiong, Y., Wood, S. and Kruszewski, J. (2006) Hydrothermal transport and deposition of rhenium under subcritical conditions revisited. *Economic Geology*, **101**, 471–478.

Yazeva, R.G. and Bochkarev, V.V. (1995) Silurian Island Arc of the Urals: Structure, Evolution, and Geodynamics. *Geotectonics, English translation*, **29**, 478–489.